Lithos 226 (2015) 65–80

Contents lists available at ScienceDirect

Lithos

journal homepage: www.elsevier.com/locate/lithos

Trace element behavior and *P*–*T*–t evolution during partial melting of exhumed eclogite in the North Qaidam UHPM belt (NW China): Implications for adakite genesis

Guibin Zhang [a,*], Yaoling Niu [b], Shuguang Song [a], Lifei Zhang [a], Zuolin Tian [a], Andrew G. Christy [c], Lei Han [a]

[a] MOE Key Laboratory of Orogenic Belts and Crustal Evolution, School of Earth and Space Sciences, Peking University, Beijing 100871, China
[b] Department of Earth Science, Durham University, Durham DH1 3LE, UK
[c] Department of Applied Mathematics, Research School of Physics and Engineering, Australian National University, Canberra, ACT 0200, Australia

ARTICLE INFO

Article history:
Received 26 May 2014
Accepted 13 December 2014
Available online 27 December 2014

Keywords:
Eclogite
Rutile
Garnet
Tonalite–trondhjemite association
Partial melting
North Qaidam UHPM belt

ABSTRACT

We have studied trace element behavior and timing of decompression melting of UHP rocks during exhumation recorded in the magmatic products, i.e., the melt phase (leucosomes), cumulate (garnetite) and residue (amphibolitized eclogite) from a single outcrop in the south Dulan area, North Qaidam UHPM belt, NW China. Two distinct episodes of partial melting are recognized. First, Grt-free tonalitic–trondhjemitic leucosome melts with higher silica crystallized at 424.0 ± 2.7 Ma. Garnets grew in the leucosome melt but fractionated out to form garnetite cumulates along with Ti-rich phases (rutile and titanite), strengthening the adakitic signature of the leucosome. Later Grt-bearing leucosome melts with an age of 412.4 ± 2.9 Ma cross-cut boudins and layers of amphibolitized eclogite. Geochemical investigation of bulk-rocks and in situ minerals verifies the genetic relationship between the amphibolitized eclogite and the tonalitic–trondhjemitic melts. Zircons from the amphibolitized eclogite have older (>700 Ma) protolith ages, with subsequent eclogite-facies metamorphism, retrograde granulite-facies overprinting and partial melting. Phase modeling and Zr-in-rutile thermometry calculations in combination with zircon geochronology reveal the evolution *P*–*T*–t path for the exhumation and the partial melting of the deeply subducted continental crust at the North Qaidam subduction zone in the Early Paleozoic.

1. Introduction

The petrogenesis of rocks in the tonalite–trondhjemite–granodiorite (TTG) association is important when assessing the early evolution of the Earth's crust, given the predominance of TTG in the Archean (Foley et al., 2000, 2002; Martin et al., 2005). Generally, these rocks have an "adakitic" signature with high Sr/Y and La/Yb ratios, consistent with melting of young and warm subducted oceanic crust (Drummond and Defant, 1990; Martin et al., 2005; Rapp et al., 2003) or partial melting of thickened lower continental crust (Castillo, 2006, 2012). Partial melting of a subalkaline metabasaltic rock (rutile-bearing hydrous eclogite) with garnet, rutile and amphibole as residual phases can account for the adakitic features (Foley et al., 2002; Rapp et al., 1991, 2003; Xiong, 2006).

Partial melting subduction-zone rocks at continental lithospheric depths is key in generating geochemical variation in related magmatic rocks (Zheng et al., 2011). This type of subduction related partial melting and the associated magmatism in ultra-high pressure metamorphic (UHPM) belts has been interpreted as resulting from exhumation-associated decompression melting of UHPM eclogitic rocks (see Song et al., 2014a and references therein). During this process, felsic leucosomes or leucogranites (e.g., Labrousse et al., 2011) are proposed to be produced under conditions of eclogite/amphibolite transition (Auzanneau et al., 2006). Although some syn- or post-collisional adakitic rocks have been investigated in Phanerozoic HP/UHP metamorphic terranes, these studies focus more only on the leucosome melts (Labrousse et al., 2011; Zheng et al., 2011). Melting of eclogite at the eclogite/granulite facies transition is rare. However, partial melting of eclogite under granulite-facies conditions in response to exhumation has been recognized in the Dulan area, North Qaidam UHPM belt (Song et al., 2014a; Yu et al., 2011).

In this paper, we report our detailed petrological, geochemical and geochronological studies of the various rock types of the melting products, with emphasis on the mineralogy and mineral compositions, especially rutile from the Dulan area, North Qaidam UHPM belt. Rutile occurs as an accessory mineral in a wide range of rocks, and is a common minor phase in high-grade metamorphic rocks (Zack et al., 2002). Rutile is known to be a major carrier for high field-strength elements (HFSEs, e.g., Ti, Nb, Ta and to a lesser extent Zr and Hf) in the restite/residuum during dehydration and melting reactions, and can thus help explain

* Corresponding author.
E-mail address: gbzhang@pku.edu.cn (G. Zhang).

http://dx.doi.org/10.1016/j.lithos.2014.12.009
0024-4937/

the Nb–Ta depletion in island arc rocks (Sun and McDonough, 1989). Consequently, many studies have examined the partitioning behavior of numerous trace elements between rutile and fluid (Green and Adam, 2003; Stadler et al., 1998) or rutile and melt phases (Foley et al., 2000; Green, 2000; Schmidt et al., 2009; Xiao et al., 2006; Xiong et al., 2005, 2011), as well as the TiO_2 solubility in the fluids (Audétat and Keppler, 2005; Manning et al., 2008) and melts (Xiong et al., 2011) of varying compositions. Titanite, another Ti-rich accessory phase, shows some geochemical similarities to rutile but exhibits higher enrichment in rare earth elements (REE) (Vuorinen and Hålenius, 2005). Green and Pearson (1987) studied Nb and Ta partitioning between Ti-rich minerals and silicate liquids. Coexistence of the two Ti-rich minerals rutile and titanite in natural rocks is uncommon, so direct studies are lacking on the roles of these two Ti-rich phases during partial melting (Xiao et al., 2011), and on HFSE distributions.

Grt-bearing and Grt-free tonalitic–trondhjemitic melts (abbreviations after Kretz, 1983) and garnetite occur as partial melting products associated with granulitized eclogite residue in South Dulan, North Qaidam UHPM belt (Song et al., 2014a). These natural samples provide an opportunity to trace partial melting processes and to study trace elemental distributions. Here, we focus on one particular outcrop for this study because this outcrop contains a complete record of melting processes and products. In the following, we report in situ elemental analyses, new bulk rock compositions and zircon U–Pb ages and Hf isotopic data for the eclogite and melting products. We discuss the melting processes with implications for the genesis of adakite and rocks of adakitic compositions.

2. Geological background and sampling

The Paleozoic North Qaidam UHPM belt lies between the Qaidam and Qilian blocks on the northern margin of the Greater Tibetan Plateau (Fig. 1a, b). The Qaidam Block is a Cenozoic intra-continental basin developed on the basement of Proterozoic Dakendaban Group gneiss (c.f. Yin and Harrison, 2000), which is dominated by metagranitic and metasedimentary rocks. The Qilian Block contains mainly Paleozoic sedimentary rocks with an underlying imbricate thrust belt of Precambrian basement that consists of granitic gneiss, pelitic gneiss, schist and marble (Song et al., 2009a). The North Qaidam UHPM belt consists of continental crustal and mantle rocks. Along this belt, eclogites are found as blocks and interlayers within the predominant para- and ortho-gneisses in several localities (e.g., Yuka, Xitieshan, and Dulan) extending from northwest to southeast for approximately 400 km (Fig. 1b). Garnet peridotite occurs at the Luliang Shan outcrops (Song et al., 2005, 2006, 2009b; Yang and Powell, 2008). The UHP metamorphism in the North Qaidam is documented by the occurrence of coesite inclusions in both eclogite and country gneiss and the diamond inclusions in garnet peridotite (see the reviews of Zhang et al., 2013 and Song et al., 2014b for more details).

The Dulan terrane is located on the eastern end of the North Qaidam UHPM belt (Fig. 1b). It is subdivided into southern and northern sub-belts (Fig. 1c, Song et al., 2003a, b; Yang et al., 2003). Rocks from these two belts show different geochemical signatures and experienced differences in thermal evolution (Song et al., 2003b; Zhang et al., 2013, 2014). The Shaliuhe relict oceanic lithology crops out in the eastern portion of this area (Fig. 1c, Zhang et al., 2005, 2008, 2009; Zhang and Zhang, 2011). In the southern Dulan sub-belt, some eclogites experienced decompression melting under the granulite-facies condition in the course of exhumation (Song et al., 2014a) although some interpreted as melting under the thickened lower crustal conditions (Yu et al., 2011). Boudins or layers of eclogites, which range in size from tens of centimeters to hundreds of meters, occur throughout the Dulan terrane. Song et al. (2014a) described the field relationships and petrography of granulitized eclogite, Grt-bearing leucosome melts and tonalitic plutons in detail. In the field, in-situ leucosomes can be observed, which are consistent with the migmatitic texture defined by Sawyer and Brown (2008) (Fig. 2a). In this study, we focus on one newly discovered outcrop (Fig. 2a), in which granulitized eclogite residue (subsequently retrogressed under amphibolite-facies condition as amphibolitized eclogite), Grt-bearing leucosome, Grt-free leucosome and garnetite are all present. The coexistence of these lithologies makes this outcrop unique. The Grt-free leucosome melts show equilibrium with the garnetite, which is cumulate crystallized from the leucosome melts (Song et al., 2014a), while the Grt-bearing

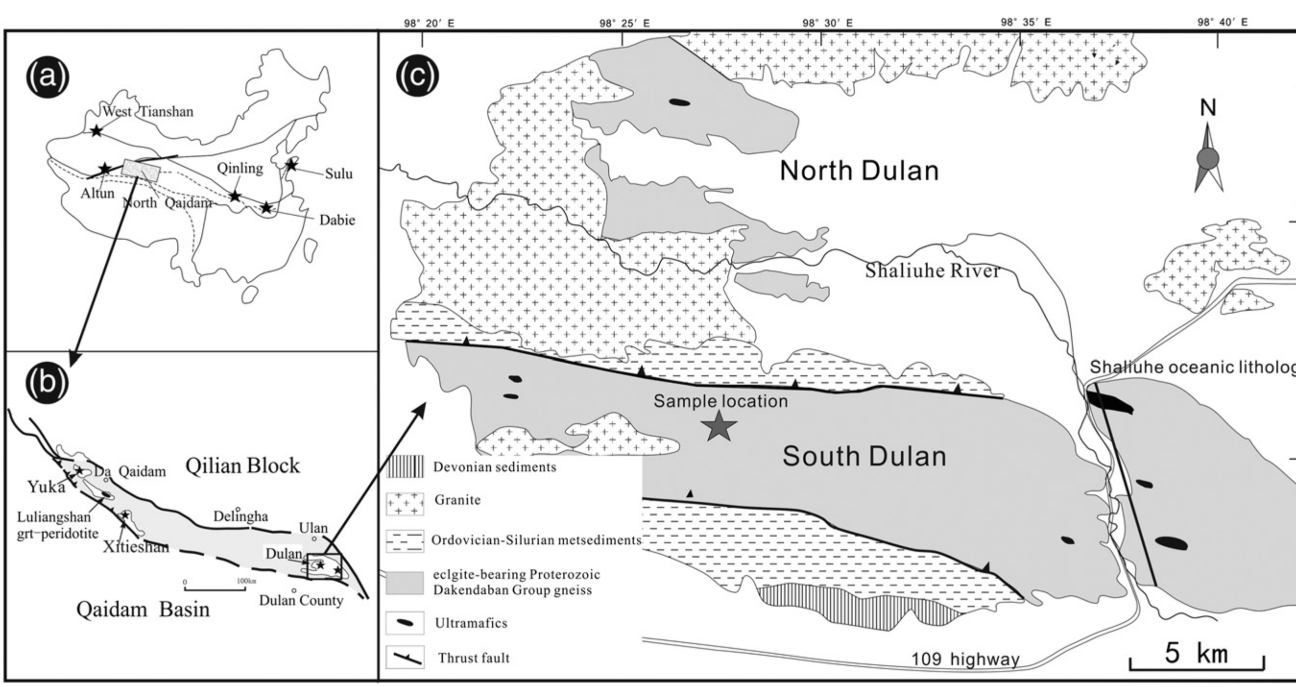

Fig. 1. Geological sketch map of Dulan terrane, North Qaidam UHPM belt, China.

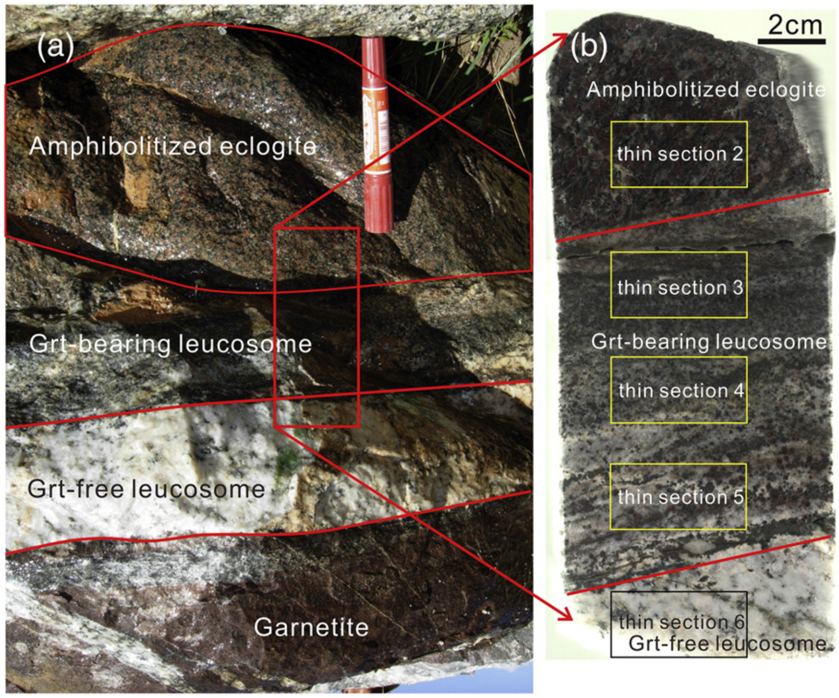

Fig. 2. Field view of the amphibolitized eclogite and leucosome melts, North Qaidam UHPM belt, China. (a) and (b) amphibolitized eclogite, garnet-bearing leucosome, tonalitic–trondhjemitic leucosome and garnetite coexisting in one outcrop. The yellow rectangles (b) represent positions of thin-sections cut and studied.

leucosome melts occur as interlayers sandwiched between Grt-free leucosome melts and granulitized eclogite residue (Fig. 2a, b).

3. Analytical methods

3.1. Mineral major and trace element analysis

Chemical compositions and elemental maps of minerals were obtained using a JEOL JXA 8800 electron microprobe at the Institute of Mineral Resources, Chinese Academy of Geological Sciences, Beijing. Operating conditions: 15 kV accelerating potential, 10 nA specimen current for compositions and mapping analysis, and 40 s counting time per composition analysis. The quantification used the ZAF correction. Both natural and synthetic crystals were used as standards for calibration. To evaluate the significance of some mineral phases (e.g. rutile, titanite, garnet, etc.) in trace elemental distribution in the garnetite, elemental mapping was performed using thin sections. The method is the same as done by Zack et al. (2002). For compositional maps, point analyses were collected over 6 h (i.e., 70 ms per point, 50 μm step width and mapping area 12 × 12 mm) with Mg, Al, K, Ca, and Fe measured by WDS and Na, Si, P and Ti measured by EDS. The modal proportions of the major mineral phases were estimated by point counting of element maps.

Trace elements in rock-forming minerals were analyzed using laser ablation ICP-MS on an Agilent 7500ce mass spectrometer at Peking University. The samples were ablated using a 193 nm ArF-excimer laser with a pulse rate of 5 Hz and a pulse energy of 50 mJ. NIST 610 glass was used as an external standard with the recommended values from Pearce et al. (1997); NIST 612 and 614 were used concurrently as monitoring standards. The data were reduced using GLITTER 4.4.2 (Macquarie University, van Achterbergh et al., 2001). Duplicate analyses of the NIST-612 glass standard implied that the precision (RSD) was 2.2% (Zr), 1.4% (Nb), 2.5% (Hf), and 2.0% (Ta), while the accuracy (RD) was 2.9% (Zr), 4.5% (Nb), 3.4% (Hf), and 12.5% (Ta).

3.2. Bulk rock major and trace elements analysis

Major element compositions of the bulk rock samples were analyzed using a RIX-2100 X-ray fluorescence (XRF) spectrometer on fused glass disks at Peking University. All of the analytical data were normalized against Chinese rock reference standard GBW07105, and the analytical uncertainties range from ±1% to ±5%. Trace element abundances of bulk rock samples were analyzed using an Agilent 7500ce ICP-MS after an acid digestion of sample powders in Teflon bombs at Peking University. The analytical details are as reported by Gou et al. (2012). Two USGS rock reference materials, BCR-2 and BHVO-2, were used to monitor analytical accuracy and precision. The accuracy was ±5% for the trace elements with abundances of ≧20 ppm and ±10% for elements with abundances of ≦20 ppm.

3.3. Zircon U–Pb dating and Hf isotopes analysis

Samples of the four lithologies (i.e., amphibolitized eclogite, Grt-bearing and Grt-free leucosome, and garnetite; Fig. 2a) were crushed and sieved for zircon separation by magnetic and heavy liquid techniques before finally being handpicked under a binocular microscope. The separated zircons and zircon standard Qinghu (159.5 ± 0.7 Ma; Li et al., 2009) were embedded in 25 mm epoxy disks and polished down to approximately half thickness. Their microstructure was examined by cathodoluminescence (CL) on a FEI Philips XL30 SFEG SEM at Peking University with a 2-min scanning time at 15 kV and 120 pA. The U, Th and Pb of the zircons from the amphibolitized eclogite, Grt-bearing and Grt-free leucosome were analyzed using a Cameca IMS 1280 SIMS at the Beijing Ion Microprobe Center, Chinese Academy of Sciences. The instrumental conditions and measurement procedures were similar to those reported by Li et al. (2009). Each measurement consisted of 7 counting cycles with the total analytical time of ~12 min. The results are given in Table 3.

Zircons from the garnetite were analyzed by LA-ICP-MS at Peking University. The analytical details are similar to those described by Yuan et al. (2004) and Gou et al. (2012). The diameter of the laser spot was 32 μm. The calibrations for elemental concentrations were carried out using NIST 610 glass as an external standard and ^{29}Si as internal standard. Plešovice zircon (337.3 ± 0.4 Ma; Sláma et al., 2008) was used as an external standard to correct for isotope fractionation effects, and Qinghu (159.5 ± 0.7 Ma; Li et al., 2009) was a monitoring standard. Squid (Ludwig, 2002) and isoplot (Ludwig, 2003) programs were used for data processing. Common Pb was corrected according to the method by Andersen (2002). The results are given in Table 4.

The zircon Hf isotopes of the Grt-free leucosome melts were analyzed using a Geolas-193 laser-ablation microprobe attached to Neptune multi-collector ICP-MS at the Institute of Mineral Resources, Chinese Academy of Geological Sciences, Beijing. The instrumental conditions and data acquisition were described by Hou et al. (2007). The results are given in Table 5.

4. Petrography and mineral chemistry

4.1. Major elements

The eclogite experienced amphibolite-facies retrogression, giving rise to the mineral assemblage of Grt + Amp + Ky + Ep + Pl + Qtz + Rt (Fig. 3a). The omphacite inclusions in kyanite suggest an eclogitic precursor with a later granulite-facies overprint producing the mineral assemblage of Grt + Cpx + Pl + Scp (Song et al., 2003a, 2014a). Rutile occurs mostly in the matrix with varying sizes and shapes (a few 10–30 μm for inclusions, 20–100 μm for matrix; Fig. 3a) coexisting with garnet and amphibole. Representative mineral compositions are given in Table 1.

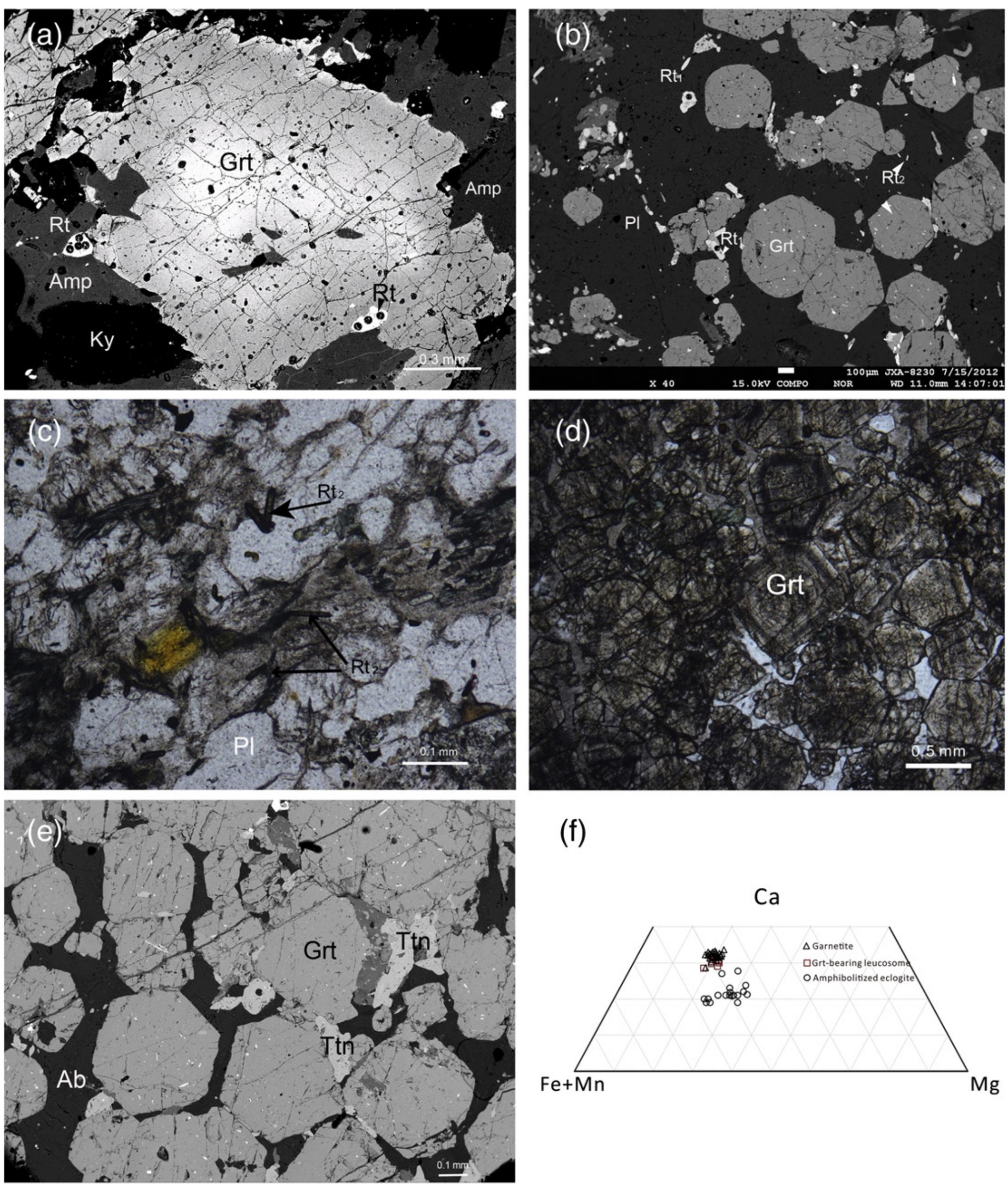

Fig. 3. Micrographs of thin-sections from different parts of the outcrops in Fig. 2b. (a) Garnet porphyroblast coexisting with amphibole, kyanite and rutile in amphibolitized eclogite; (b) Fine-grained euhedral to subhedral garnet crystals coexisting with a felsic matrix and two generations of rutile in garnet (Grt)-bearing leucosome; (c) New-growth rutile (Rt_2) in Grt-free leucosome; (d) and (e) Garnet crystals coexisting with albite and titanite in garnetite; (f) Comparison of garnet compositions from amphibolitized eclogite, Grt-bearing leucosome and garnetite.

Table 1
Representative mineral compositions of the amphibolitized eclogite, leucosomes and garnetite, South Dulan, North Qaidam UHPM belt, China.

	Amphibolitized eclogite					Grt-bearing leucosome				Grt-free leucosome			Garnetite		
	Grt		ep	hb	mu	chl	fsp	grt	ep	ep	fsp	chl	grt	ttn	fsp
	Rim	Core													
SiO_2	38.75	38.50	39.38	42.34	50.03	27.37	63.16	38.86	37.37	37.42	63.74	29.02	37.61	29.74	66.16
TiO2	0.02	0.04	0.38	0.50	0.00	0.32	0.00	0.14	0.00	0.96	0.00	0.06	0.49	37.20	0.00
Al_2O_3	21.27	21.20	29.13	16.32	28.68	20.14	23.22	21.35	22.74	23.77	23.19	18.78	20.57	2.77	20.78
Cr_2O_3	0.01	0.01	0.02	0.02	0.08	0.13	0.00	0.00	0.02	0.03	0.00	0.07	0.06	0.01	0.00
FeO	22.00	26.79	5.78	15.10	4.31	21.55	0.10	23.51	14.12	12.04	0.07	20.70	23.52	0.66	0.02
MnO	0.40	0.35	0.00	0.09	0.02	0.10	0.03	0.26	0.05	0.09	0.00	0.08	0.15	0.00	0.01
MgO	8.27	6.43	0.26	10.61	2.60	19.80	0.00	7.58	0.01	0.02	0.00	20.19	4.83	0.07	0.00
CaO	8.47	6.91	23.72	11.52	0.33	0.15	4.49	8.40	23.07	22.62	4.25	0.10	12.58	28.68	1.32
Na_2O	0.03	0.01	0.02	1.68	0.29	0.00	9.26	0.03	0.02	0.08	9.33	0.06	0.05	0.05	11.29
K_2O	0.01	0.00	0.00	0.92	9.35	0.00	0.36	0.00	0.00	0.01	0.30	0.03	0.03	0.00	0.03
Totals	99.23	100.24	98.69	99.10	95.69	89.56	100.62	100.13	97.40	97.04	100.88	89.09	99.89	99.18	99.61
Oxygen	12.00	12.00	12.50	23.00	11.00	14.00		12.00	12.50	12.50	8.00	14.00	12	11.00	
Si	2.98	2.98	3.01	6.19	3.31	2.76	11.13	2.98	2.97	2.97	11.19	2.92	2.92	2.16	11.67
Ti	0.00	0.00	0.02	0.05	0.00	0.02	0.00	0.01	0.00	0.06	0.00	0.01	0.03	2.03	0.00
Al	1.93	1.94	2.62	2.81	2.24	2.39	4.82	1.93	2.13	2.23	4.79	2.23	1.89	0.24	4.32
Cr	0.00	0.00	0.00	0.00	0.00	0.01	0.00	0.00	0.00	0.00	0.00	0.01	0.00	0.00	0.00
Fe^{3+}	0.12	0.09	0.33	0.00	0.16	0.03	0.01	0.10	0.93	0.71	0.01	0.00	0.22	0.00	0.00
Fe^{2+}	1.30	1.64	0.04	1.85	0.08	1.78	0.00	1.41	0.01	0.09	0.00	1.74	1.31	0.04	0.00
Mn	0.03	0.02	0.00	0.01	0.00	0.01	0.00	0.02	0.00	0.01	0.00	0.01	0.01	0.00	0.00
Mg	0.95	0.74	0.03	2.31	0.26	2.97	0.00	0.87	0.00	0.00	0.00	3.03	0.56	0.01	0.00
Ca	0.70	0.57	1.94	1.80	0.02	0.02	0.85	0.69	1.96	1.93	0.80	0.01	1.05	2.23	0.25
Na	0.00	0.00	0.00	0.48	0.04	0.00	3.17	0.00	0.00	0.01	3.18	0.01	0.01	0.01	3.86
K	0.00	0.00	0.00	0.17	0.79	0.00	0.08	0.00	0.00	0.00	0.07	0.00	0.00	0.00	0.01
Sum	8.00	8.00	8.00	15.82	6.90	10.00	20.06	8.00	8.01	8.01	20.03	9.97	8.00	6.70	20.10

The ratio Fe^{2+}:Fe^{3+} was estimated so as to obtain 8 cations per 12 oxygens for garnet.

The backscattered electron (BSE) images and major element compositions of garnet show zoning from core to rim (Fig. 3a, Table 1) with almandine decrease (56 to 44 mol%), pyrope increase (23 to 33 mol%,) and grossular increase (19 to 28 mol%) (Table 1, Fig. 3f). The amphibole is an Al-rich calcium amphibole in the classification of Hawthorne et al. (2012); recalculation of the formula gives the species as pargasite or tschermakite, depending on the Fe^{2+}/Fe^{3+} ratio that is assumed.

The Grt-bearing leucosome melt crystallized to an assemblage of Fsp + Qtz + Rt + Ep (Aln) + Ttn + Grt (Fig. 3b). The garnet occurs as euhedral/subhedral crystals with grain sizes below 1 mm (Fig. 3b). The samples show some garnet-rich layers (Fig. 2b). The garnet crystals have homogeneous compositions with more grossular and less pyrope than garnet of the amphibolitized eclogite (Table 1, Fig. 3f). The Grt-free leucosome melts crystallized to a tonalitic–trondhjemitic assemblage of Fsp + Qtz + Rt + Chl + Ttn (Fig. 3c). In the Grt-bearing and Grt-free leucosome melts, two generations of rutile can be recognized: relict vs neocryst. The relict rutile grains are similar in shape and size to those in the amphibolitized eclogite (Fig. 3b; Rt_1). Neocrystallized rutile occurs as inclusions within the garnet (Fig. 3b; Rt_2) or very tiny, rod-like crystals coexisting with the matrix feldspar (An 6–22) and quartz (Fig. 3c; Rt_2).

The garnetite is mainly composed of euhedral granular garnet (~90 vol.%, 3–5 mm in grain size) with minor interstitial Ab + Ttn + Rt + Ep (Fig. 3d). The garnet is homogeneous in major elements (but not trace elements: see below), with compositions similar to that of the Grt-bearing leucosome (Table 1, Fig. 3f). A few rutile grains occur in the matrix and coexist with the garnet. The titanite also occurs as large crystals coexisting with the garnet (Fig. 3e).

4.2. Garnet trace elements

Rare-earth element (REE) patterns and other trace elements for garnet from the amphibolitized eclogite, leucosome and garnetite are all very different (Fig. 4). Garnet from the amphibolitized eclogite contains 1–12 ppm Zr and 6–24 ppm Y; it is characterized by strong LREE depletion and HREE enrichment ($La_N/Yb_N < 0.01$) with no obvious core-to-rim zoning (Fig. 4a). In contrast, the garnet from the Grt-bearing leucosome contains 20–150 ppm Zr and 20–65 ppm Y and is very weakly zoned. Its chondrite-normalized REE pattern shows LREE and MREE enrichment (Fig. 4b) compared with the garnets from amphibolitized eclogite. The distinctive, strongly REE-zoned garnet from the garnetite has been analyzed in detail (Fig. 4c). The laser ablation data for the garnet cores show Ti contents that are always higher than the EMP data due to the influence of these rutile inclusions. However, the REE contents of the rutile are always below the detection limit (Appendix A). Thus, the rutile has a very limited influence on the REE compositions of garnet. All of the garnets from the garnetite display rimward decrease in Zr, Y, MREE and HREE (Fig. 4c). The maximum core Zr contents (205 ppm) decrease to 28 ppm in the rim, while the Y core contents are 100 ppm, decreasing to 17 ppm in the rim (Appendix A). The Gd contents decrease from ~110 to 30× chondrite from core to rim, while the Yb contents decrease from 30 to 2× chondrite, and (Gd_N/Yb_N) varies accordingly from 4.1 to 13.7, Fig. 4c). A negative Eu anomaly decreases slightly in magnitude from Eu/Eu* = 0.86 in the core to 0.71 in the rim.

4.3. Rutile trace elements and Zr-in-rutile thermometry

More than 200 rutile grains were analyzed from thin sections of amphibolitized eclogite (thin Section 2), Grt-bearing leucosome (thin Sections 3–5), Grt-free leucosome (thin Section 6) and garnetite (Fig. 2b, Appendix B). Rutile incorporates most high field-strength elements, especially Nb and Ta (eg., Zack et al., 2002). The rutile from the amphibolitized eclogite has relatively low Nb and Ta contents (96–340 ppm for Nb, 3.4–17.9 ppm for Ta) and high Nb/Ta ratios (19.0–65.6) (Fig. 5). Only a few neocrystallized rutile grains from leucosome melts were large enough for laser ablation analysis. Both relict and neocrystallized rutile grains have the same high Nb and Ta contents (Nb = 331–4594 (most over 2000) ppm, Ta = 89.7–367 ppm) and lower Nb/Ta ratios than rutile in the amphibolitized eclogite (Fig. 5). The rutile grains from the garnetite have high Nb and Ta contents with low Nb/Ta ratios, a signature similar to that of the leucosome

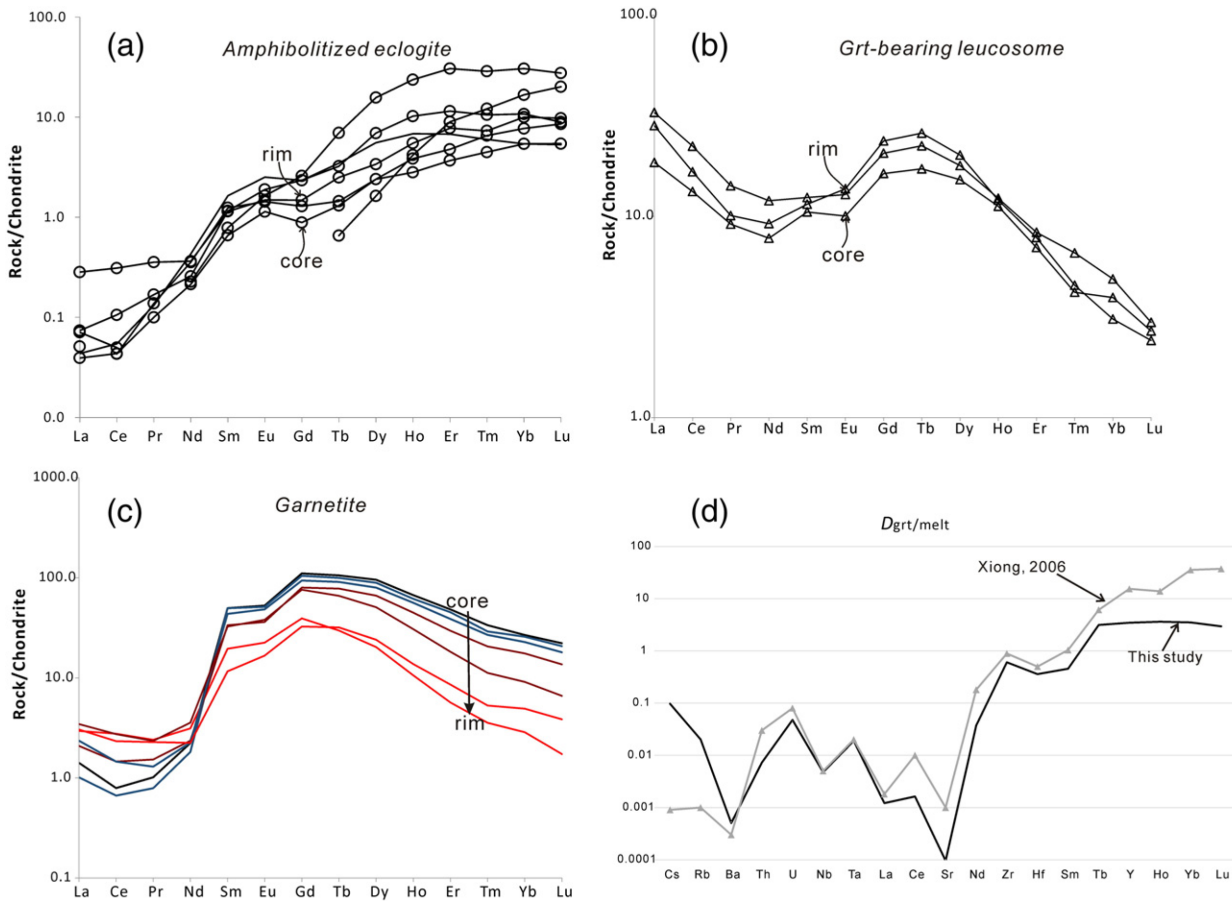

Fig. 4. Chondrite-normalized REE patterns of the garnet in the amphibolitized eclogite (a), in Grt-bearing leucosome (b), and in garnetite (c) from South Dulan, North Qaidam UHPM belt, China, and comparison of garnet/melt partition coefficients between experimental data (Xiong, 2006) and our observed data (d).
Chondrite values are from Sun and McDonough (1989).

melts (Nb = 1095–3383 ppm, Ta = 81.4–298 ppm, Nb/Ta: 8.2–15.6; Fig. 5).

Zr concentrations in rutile show an obvious decrease from Grt-free leucosome (thin Section 6: 1001 ± 43 ppm, 64 spots) to Grt-bearing leucosome (thin Section 5: 633 ± 95 ppm, 37 spots; thin Section 4: 480 ± 80 ppm, 21 spots; thin Section 3: 350 ± 19 ppm, 72 spots) and to the amphibolitized eclogite (thin Section 2: 325 ± 22 ppm, 72 spots) (Appendix A). From these data, temperatures can be estimated using the equation of Tomkins et al. (2007) if pressure is known. For rutile grains in the Grt-free leucosome, the actual pressure at which the rutile formed (or the melt crystallized) is difficult to estimate (G.B. Zhang et al., 2010; J.X. Zhang et al., 2010). However, Song et al. (2014a) proposed that the partial melting was triggered by decompression at the granulite-facies conditions and that the Grt-free leucosome

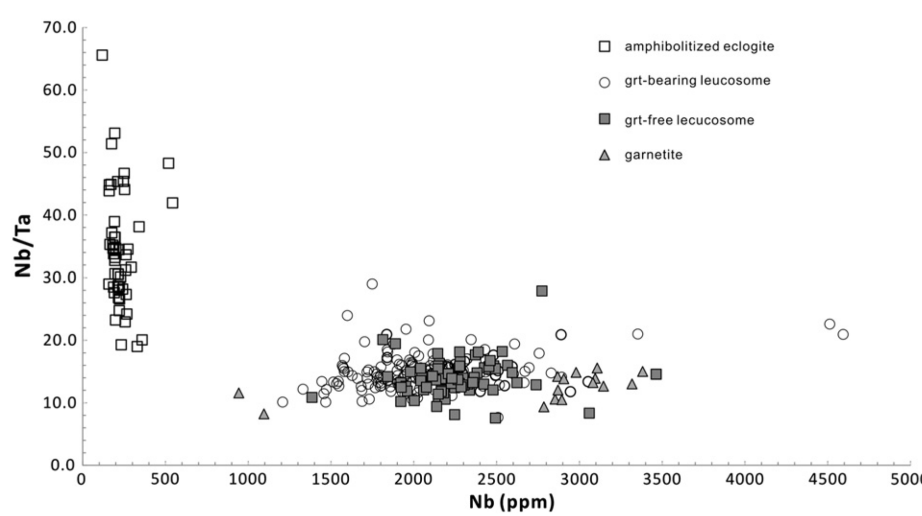

Fig. 5. Nb (ppm) vs Nb/Ta for the rutile crystals in the amphibolitized eclogite, Grt-bearing and Grt-free leucosome, and garnetite from South Dulan, North Qaidam UHPM belt, China.

was generated first. Therefore, for the partial melting products, a pressure was adopted corresponding to granulite-facies *P–T* conditions constrained by the index mineral assemblages and geothermobarometry (Song et al., 2003a, 2014a) ($P = 18–20$ kbar, Grt-Cpx-Pl-Qtz geothermobarometers with about 3 kbar uncertainty, Ellis and Green, 1979; Powell, 1985). For rutile grains in the amphibolitized eclogite, pressure was constrained by Grt-Amp-Pl-Qtz geobarometry (Kohn and Spear, 1990) to be $P = 11–13$ kbar, noting that the rutile can record the conditions of the amphibolite-facies overprint during exhumation (G.B. Zhang et al., 2010). Application of the Tomkins et al. (2007) geothermometer to the Grt-free leucosome then gave a $T = 801 \pm 10$ °C (using the weighted average Zr $= 1001 \pm 43$ ppm), while the amphibolitized eclogite gave a $T = 665 \pm 10$ °C. These data indicate that partial melting started at approximately 800 °C and that melt was present down to approximately 660 °C. During this process, the leucosome melts in Fig. 2a crystallized.

5. Bulk rock geochemistry

The major and trace element compositions of selected amphibolitized eclogite, Grt-bearing and Grt-free leucosome and garnetite samples from the outcrop of Fig. 2a are given in Table 2.

As reported by Song et al. (2014a), the amphibolitized eclogite is characterized by lower SiO_2 (~42 wt.%) and TiO_2 (0.51–0.63 wt.%), and higher FeO (~14 wt.%), MgO (~6 wt.%) and CaO (12.29–12.74 wt.%) relative to typical mafic rock compositions. It shows obvious HREE depletion and relatively flat LREE compared with the present-day N-MORB (Sun and McDonough, 1989; Fig. 6a). In the primitive-mantle-normalized spidergram (Fig. 6b), the amphibolitized eclogites are strongly enriched in Pb and Sr but depleted in high field-strength elements (HFSE) such as Nb, Ta, Zr, Hf and to a lesser extent Ti. The subchondritic ratios of Nb/Ta (13) and Zr/Hf (27–32) suggest that the protolith has undergone partial melt extraction, since Nb and Zr are more incompatible than Ta and Hf during melting (Niu, 2004). This is consistent with the granulitized eclogite being the refractory residue complementary to the partial melts represented by the leucosomes (Song et al., 2014a).

All of the leucosome melts are Al- and Na-rich and K-poor, with high Sr/Y ratios (Table 2). Geochemically, these melts resemble modern adakites (Song et al., 2014a; Yu et al., 2011). The Grt-bearing leucosome has intermediate SiO_2 (52.50–55.23 wt.%), lower FeO (4.22–5.96 wt.%), MgO (1.55–2.43 wt.%), and CaO (5.17–6.60 wt.%), and higher Na_2O (5.50–6.57 wt.%) and TiO_2 (1.40–1.96 wt.%). The Grt-bearing leucosomes are also strongly enriched in LREE ($La_N/Yb_N = 19.35–205.6$) (Fig. 6c) with obvious Zr, Hf and Pb, Sr enrichments relative to relevant REEs (Fig. 6d). In contrast, the Grt-free leucosomes contain higher SiO_2 (70.70–72.31 wt.%) and lower FeO (0.30–0.43 wt.%), MgO (0.22–0.29 wt.%) and CaO (2.41–2.80 wt.%). Their REE patterns show an obvious positive Eu anomaly ($Eu/Eu^* = 2.62–3.06$) and strong enrichment in LREE ($La_N/Yb_N = 233.6–476.0$) (Fig. 6c). The Grt-free leucosomes are enriched in Pb, Sr, Zr and Hf, to a greater degree than the Grt-bearing leucosome, relative to the neighboring elements in the spidergram (Fig. 6d).

The major element composition of garnetite is close to that of monomineralic garnet, as expected from the modal mineralogy. However, a very strong enrichment in LREE ($La_N/Yb_N = 71.13–82.36$) is observed (Fig. 6e). The garnetite shows a complementary depletion in Pb, Sr, Zr and Hf (Fig. 6f), which supports the origin of the garnetite as a cumulate from the Grt-free leucosome. This model is also consistent with the observed depletion of Th in Grt-free leucosome, but mild enrichment in Grt-bearing leucosome (Fig. 6d) and strong enrichment in garnetite (Fig. 6f). The garnetite also shows a weak negative Eu anomaly ($Eu/Eu^* = $ ~0.8), complementary to the positive anomaly in the Grt-free leucosome. Note that contrary to common expectation, the garnetite has low, not high, HREE/LREE (Fig. 6e, f). This is in fact consistent with the garnetite being of cumulate origin crystallized from HREE-poor adakitic melts such as the Grt-free leucosomes.

6. Zircon geochronology and Hf isotopes

6.1. Zircon U–Pb dating

Zircons separated from the four domains (amphibolitized eclogite, Grt-bearing and Grt-free leucosomes, and garnetite Fig. 2d) are dated (Table 3).

Most zircon crystals from the amphibolitized eclogite are subhedral, rounded and 80–150 μm in diameter (Fig. 7a). Some zircon grains show distinct cores and rims in the CL images (Fig. 7a). The cores show obvious dark and weak cloudy-zoned or fir-tree zoning CL patterns, while the rims are characterized by stronger luminescence. A few inclusions of garnet, omphacite and rutile have been identified in the zircon cores. The age data for the zircon are dispersed. Three inherited zircon cores were older than 700 Ma (Fig. 7a). In addition, three zircon age groups are distinguished. Four zircon cores yielded ^{204}Pb-corrected $^{206}Pb/^{238}U$ ages ranging from 439.5 ± 6.5 Ma to 464.7 ± 6.9 Ma with an average of 451 ± 17 Ma (Fig. 7a). Zircon rims and a few neocrystallized zircon grains have mean ages of 415.3 ± 4.7 Ma, while the other four grains gave a younger mean age of 395 ± 12 Ma (Table 3, Fig. 7a).

Most zircon grains in the Grt-bearing leucosomes have a euhedral, elongate shape with length/width ratios of 2–4. The CL images show well-developed oscillatory growth zoning (Fig. 7b). Most of the analyses (Table 3) show variable U contents (222–543 ppm) and variable Th/U ratios (0.297–0.653). Seventeen analyses yielded ^{207}Pb-corrected $^{206}Pb/^{238}U$ ages ranging from 425.8 ± 6.3 Ma to 397.1 ± 5.9 Ma, defining a Concordia age of 412.4 ± 2.9 Ma (Fig. 7b).

Zircon grains from the Grt-free leucosomes show morphologies similar to those of the Grt-bearing leucosomes (Fig. 7c), with much higher U (506–3075 ppm) and lower Th/U (0.067 to 0.148; Table 3). Eighteen analyses yielded ^{207}Pb-corrected $^{206}Pb/^{238}U$ ages ranging from 411.5 ± 6.1 Ma to 434.1 ± 6.4 Ma, defining a Concordia age of 424.0 ± 2.7 Ma (Fig. 7c). Zircon from the garnetite also shows magmatic features, defining a Concordia age of 419.2 ± 2.1 Ma (Table 4, Fig. 7d).

6.2. Zircon Hf isotopes

Zircon grains from the Grt-free leucosomes were analyzed for Hf isotopes (Table 5), giving initial $^{176}Hf/^{177}Hf$ ratios of 0.282332–0.282520 (ε_{Hf} (424 Ma) $= -6.3$ to 0.4) and old model ages of $T_{DM1} =$ 1011–1268 Ma.

7. Phase equilibrium modeling

To discuss the causes and tectonic context of the partial melting in the investigated samples, a *P–T* pseudosection was calculated for the amphibolitized eclogite composition in the NCKFMASHTO system using the THERMOCALC 3.33 software (Powell et al., 1998; updated July 2009) with the internally consistent thermodynamic data set (file tcds55.txt) by Holland and Powell (1998; updated Nov. 2003). Here, the original eclogite is assumed to have the same major-element bulk composition as its amphibolitized counterpart, as reported by Song et al. (2003b). The following solid–solution models have been used for the phases considered in the calculation: amphiboles (Diener et al., 2007), clinopyroxene (Green et al., 2007), chlorite (Holland et al., 1998), garnet (White et al., 2007), epidote and talc (Holland and Powell, 1998), plagioclase (Holland and Powell, 2003), phengitic muscovite (Coggon and Holland, 2002), ilmenite (White et al., 2000) and the melt (modified from White et al., 2007). Lawsonite, kyanite, rutile, titanite and quartz/coesite are treated as pure end-member phases. In these assemblages, the *P–T* uncertainties on the isopleths calculated with THERMOCALC are 1–2 kbar and 8–10 °C (2σ level). However, such uncertainties should be considered a minimum, as they are propagated from the uncertainties on the enthalpy alone and do not include other sources of uncertainty.

Table 2
Major and trace elemental compositions of the amphibolitized eclogite, leucosomes and garnetite, South Dulan, North Qaidam UHPM belt, China.

Sample	Amphibolitized eclogite		Grt-bearing leucosome						Grt-free leucosome					Garnetite			
	1	2	3	4	5	3–5–1	3–5–2	7–1	6–1	6–2	6–4	6–5	6–6	7–2	7–3	7–4	7–5
Major elements (wt.%)																	
SiO_2	42.81	42.32	52.5	54.69	53.04	54.91	55.16	55.23	71.11	70.64	72.31	70.66	72.57	40.07	39.1	39.6	39.53
TiO_2	0.63	0.51	1.96	1.4	1.68	1.43	1.48	1.76	0.28	0.23	0.36	0.3	0.25	3.14	3.33	3.08	3.18
Al_2O_3	21.39	21.68	21.22	21.9	21.69	21.47	21.77	19.81	16.03	16.42	15.51	16.18	16.22	19.14	18.6	18.92	19.3
Cr_2O_3	0.01	0.01	<0.01	<0.01	<0.01	<0.01	0.01	0.01	<0.01	<0.01	<0.01	<0.01	<0.01	0.01	0.01	0.01	0.01
Fe_2O_{3T}	14.16	14.15	4.94	4.52	5.96	4.25	4.79	4.22	0.33	0.3	0.3	0.35	0.43	19.85	19.1	20.05	19.9
MnO	0.23	0.24	0.05	0.05	0.07	0.05	0.05	0.04	<0.01	<0.01	<0.01	<0.01	<0.01	0.16	0.15	0.16	0.16
MgO	5.94	5.81	2.41	1.55	2.26	1.9	1.75	2.43	0.23	0.22	0.25	0.25	0.29	4.1	4.13	4.09	4.07
CaO	12.29	12.74	6.2	5.51	6.17	5.87	5.17	6.6	2.69	2.8	2.42	2.41	2.76	11.68	11.81	11.43	12.09
Na_2O	1.35	1.22	5.5	6.4	5.63	6.12	6.57	6.09	5.59	5.54	5.66	6.2	5.57	1.3	1.29	1.24	1.1
K_2O	0.3	0.34	0.74	0.62	0.63	0.61	0.87	0.78	0.81	0.91	0.88	0.77	0.84	0.1	0.09	0.11	0.12
P_2O_5	0.341	0.351	0.539	0.364	0.446	0.432	0.389	0.421	0.035	0.034	0.033	0.035	0.035	0.556	0.637	0.54	0.552
SrO	0.1	0.11	0.25	0.25	0.18	0.23	0.17	0.22	0.15	0.16	0.13	0.1	0.15	0.03	0.03	0.03	0.04
BaO	0.01	0.01	0.04	0.03	0.03	0.03	0.03	0.05	0.02	0.02	0.02	0.01	0.02	0.01	0.01	0.01	0.01
LOI	0.42	0.53	2.24	1.57	1.26	1.45	1.73	1.35	1.13	1.05	0.98	1.04	0.88	0.13	0.01	0.18	0.04
Total	99.99	100	98.6	98.85	99.05	98.75	99.94	99	98.4	98.32	98.86	98.3	100	100	98.28	99.08	100
Trace element (ppm)																	
Co	35	34.6	12.1	13.4	9.4	10.4	12.5	11	3.1	1.8	2.3	2.5	3.6	28.2	27	28.1	27.1
Cs	0.52	0.5	1.27	0.64	0.63	0.8	0.82	0.36	0.52	0.58	0.53	0.49	0.48	0.16	0.15	0.15	0.17
Ga	24.7	26.9	22.8	21.5	21.5	22.1	22.5	23	15.3	15.5	14.1	15.2	15.2	21.1	20.5	20.8	21.9
Mo	<2	<2	<2	<2	<2	<2	<2	<2	<2	<2	<2	<2	<2	<2	<2	2	<2
Sn	1	1	4	3	4	3	3	5	1	1	1	1	1	6	6	6	5
Tl	<0.5	<0.5	<0.5	<0.5	<0.5	<0.5	<0.5	<0.5	<0.5	<0.5	<0.5	<0.5	<0.5	<0.5	<0.5	<0.5	<0.5
V	341	424	75	44	68	78	54	86	9	8	12	13	14	111	110	108	109
W	1	1	3	2	3	3	3	2	1	1	1	1	1	2	1	2	2
Cr	<10	<10	10	10	20	10	10	20	<10	<10	<10	<10	<10	<10	10	<10	<10
Rb	9.3	10.7	32.5	15.3	19.3	18.4	33.7	10.6	11	11.8	15.7	19.1	11.9	4.5	3.7	4.5	5
Ba	65.7	71.7	407	301	256	265	250	420	230	249	217	176	238	16.9	11.1	15.4	18.2
Th	0.85	0.37	83.1	5.87	5.59	13.85	6.93	6.75	0.08	0.12	0.12	0.23	0.1	20.3	23.6	19.3	20.1
U	0.4	0.38	5.25	2.7	1.4	2.5	2.74	1.28	0.27	0.22	0.44	0.3	0.37	4.98	5.61	4.83	4.87
Nb	1.3	0.8	34.6	25.6	30.8	25.7	27.1	22.2	3.9	3.5	5.4	3.7	4.4	21.4	23	21.4	21.3
Ta	0.1	<0.1	2.8	2	2.3	2.1	2.2	1.8	0.3	0.3	0.5	0.3	0.4	1.9	2.2	1.9	1.9
La	11.4	9.3	117.5	23.6	23.2	37.1	28.9	33.8	6.1	6.2	4.4	7.2	5.6	63.2	71.4	58.8	64.3
Ce	25.3	20.9	275	47.2	46.9	73.8	53.3	84.2	7.7	8.6	5.7	9.2	7.3	200	225	189	200
Pr	3.36	2.85	26.7	5.21	5.27	8.38	6.06	10.85	0.73	0.85	0.56	0.86	0.72	25.7	29.2	24.7	25.5
Sr	986	1065	2490	2470	1775	2150	1685	2180	1580	1655	1315	1090	1595	301	310	256	416
Nd	15.9	13.6	91.9	20.6	22.1	31.8	23.7	46.9	2.9	3.2	2.2	3.3	2.8	112	124	108.5	109
Zr	16	19	911	684	453	477	592	150	48	30	88	48	66	258	252	246	251
Hf	0.6	0.6	20.8	14.9	9.6	11.6	13.9	3.8	1.1	0.8	2.1	1.2	1.5	5.8	6	5.6	5.7
Sm	3.28	2.76	13	3.91	5.28	5.24	4.38	8.88	0.35	0.42	0.31	0.38	0.35	24.3	25.9	23.8	24.3
Eu	1	0.94	2.27	1.27	1.54	1.33	1.29	1.87	0.25	0.26	0.23	0.23	0.23	5.83	5.94	5.69	5.76
Gd	2.84	2.5	6.52	3.63	5.65	4.05	3.95	5.1	0.19	0.23	0.17	0.19	0.2	19.35	19.55	19.35	19.15
Tb	0.38	0.31	0.73	0.43	0.69	0.53	0.54	0.51	0.024	0.023	0.017	0.022	0.025	2.18	2.14	2.18	2.18
Dy	2.12	1.84	2.95	2.11	3.3	2.19	2.42	1.99	0.08	0.09	0.05	0.06	0.08	7.74	7.87	7.88	7.83
Y	10.3	9.1	10.3	8.4	13.1	8.1	9.4	7.8	0.31	0.30	0.19	0.22	0.26	22.9	22.8	22.8	22.7
Ho	0.41	0.35	0.37	0.29	0.47	0.3	0.34	0.27	0.01	0.01	0.01	0.01	0.01	0.83	0.84	0.8	0.81
Er	1.1	0.95	0.66	0.63	1.11	0.64	0.76	0.63	0.025	0.025	0.014	0.014	0.019	1.4	1.53	1.36	1.34
Tm	0.15	0.14	0.08	0.08	0.14	0.08	0.1	0.08	0.003	0.003	0.002	0.003	0.004	0.14	0.15	0.14	0.13
Yb	0.96	0.81	0.41	0.42	0.86	0.42	0.53	0.47	0.019	0.019	0.011	0.011	0.012	0.59	0.72	0.57	0.56
Lu	0.14	0.12	0.06	0.06	0.12	0.06	0.07	0.07	0.003	0.002	0.001	0.002	0.003	0.07	0.09	0.07	0.06
Eu*	1.00	1.09	0.75	1.03	0.86	0.88	0.95	0.85	2.96	2.56	3.06	2.62	2.66	0.82	0.81	0.81	0.82
$[Gd/Yb]_N$	2.45	2.55	13.16	7.15	5.43	7.98	6.17	8.98	8.39	10.08	12.30	14.49	13.33	27.13	22.46	28.08	28.29
$[La/Sm]_N$	2.24	2.18	5.83	3.90	2.84	4.57	4.26	2.46	11.25	9.53	9.16	12.23	10.33	1.68	1.78	1.59	1.71
$[La/Yb]_N$	8.52	8.24	205.6	40.31	19.35	63.36	39.11	51.58	233.6	235.6	276.1	476.0	323.7	76.84	71.13	74.00	82.36
Sr/Y			241.7	294.0	135.5	265.4	179.3	279.5	5050	5546	7081	5023	6053				

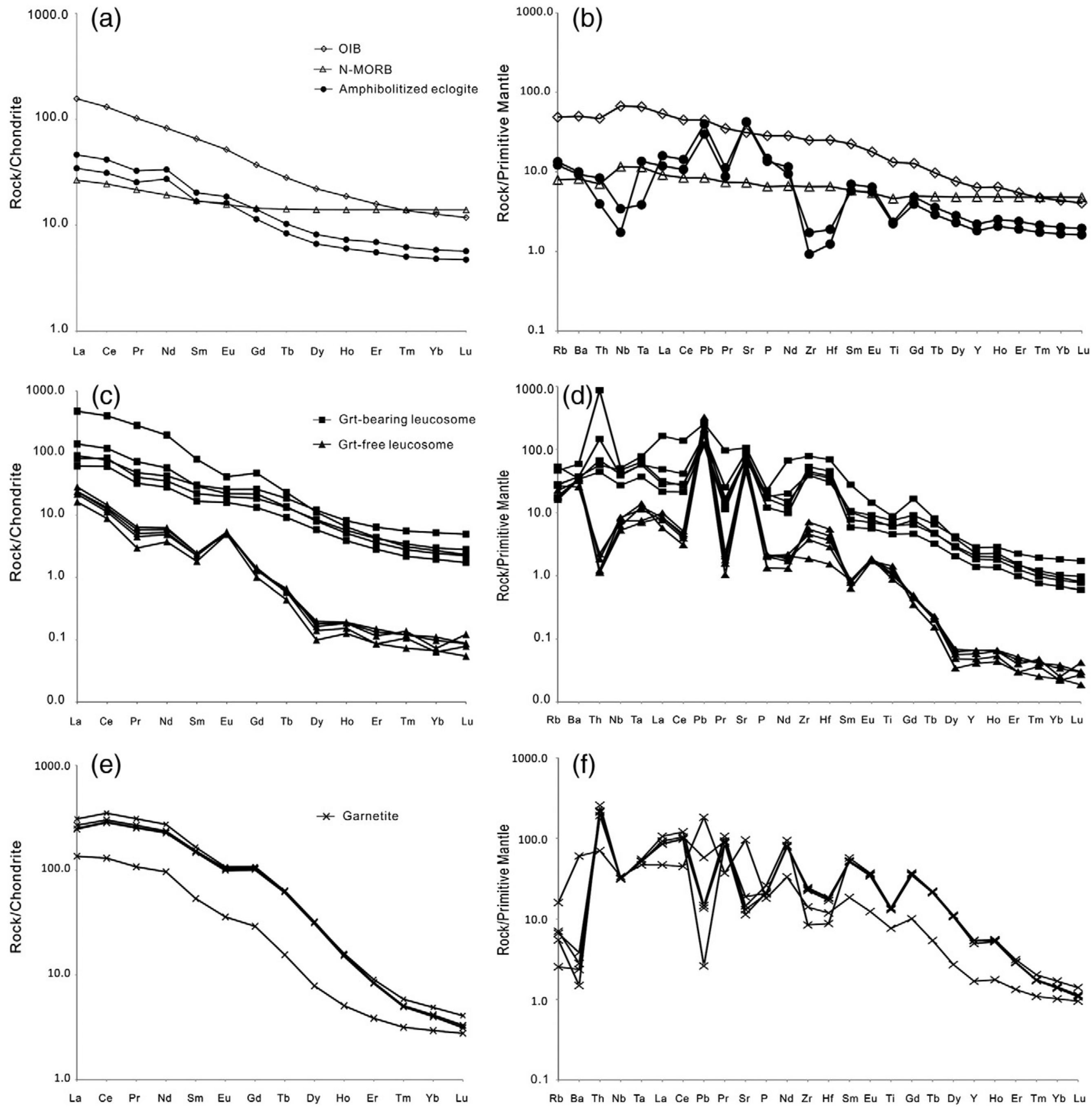

Fig. 6. Chondrite-normalized REE patterns and primitive mantle-normalized spidergrams of amphibolitized eclogite (a and b), Grt-bearing and Grt-free leucosome (c and d), and garnetite (e and f) from South Dulan, North Qaidam UHPM belt, China.
Chondrite and primitive mantle values are from Sun and McDonough (1989).

As shown in Fig. 9, the peak metamorphic conditions are predicted to be 29–33 kbar at 729–768 °C (Song et al., 2003a), which were calculated using the Grt-Omph-Phn-Ky geothermobarometer (Krogh Ravna and Terry, 2001) for a fresh kyanite eclogite from the same location as the investigated samples. The post-peak decompression path is deduced using the temperature constrained by the Zr-in-rutile thermometer and garnet compositional isopleths. We plot the weighted average Zr concentrations of rutile in the thin sections of Grt-free leucosome and amphibolitized eclogite on the Zr-in-rutile contours in the *P*–*T* diagram (Fig. 9). In three thin sections from the Grt-bearing leucosome, the rutile grains have Zr concentrations between those of Grt-bearing leucosome and amphibolitized eclogite. The zircon U–Pb data also indicate that the Grt-bearing leucosome solidified between the formation of the Grt-free leucosome production and the amphibolite-facies retrogression of the eclogite. Therefore, the weighted average Zr concentrations for their rutile grains are plotted between these two points (Fig. 9), which constrain the start- and end-points of the partial melting. In combination with the zircon geochronology data, we obtain a *P*–*T*–t path for the thermal evolution during the melting process (Fig. 9) that first crosses the saturated solidus at ~20 kbar and 800 °C, and then generates ~10% melt. Further along the decompression path during cooling, crystallization is favored rather than melt production. Garnet is a liquidus phase throughout. The grossular and pyrope contents of the garnet in the Grt-bearing leucosomes and the garnetite yield *P*–*T* conditions of 14–16 kbar and 710–750 °C, similar to the saturated solidus.

Table 3
Zircon U, Th and Pb data for the amphibolitized eclogite, leucosomes and garnetite, South Dulan, North Qaidam UHPM belt, China.

Sample spot #	[U] ppm	[Th] ppm	[Pb] ppm	Th/U meas	$^{207}Pb/^{235}U$	±1σ (%)	$^{206}Pb/^{238}U$	±1σ (%)	r	207-corr age (Ma)	±1σ
Amphibolitized eclogite											
10SD-001@1	260	15	19	0.056	0.51870	2.72	0.0674	1.52	0.56045	419.8	6.3
10SD-001@11	356	166	28	0.465	0.51165	2.25	0.0667	1.50	0.66763	416.0	6.1
10SD-001@12	250	77	21	0.310	0.56428	2.75	0.0722	1.51	0.54872	449.1	6.7
10SD-001@13	316	1	[22]	0.004	0.51259	2.34	0.0667	1.50	0.64190	415.6	6.1
10SD-001@15	196	13	14	0.064	0.49743	2.59	0.0646	1.50	0.57965	403.0	6.0
10SD-001@16	90	17	7	0.189	0.51470	3.41	0.0657	1.57	0.45977	409.1	6.3
10SD-001@18	115	39	9	0.335	0.50154	2.91	0.0672	1.50	0.51543	419.7	6.2
10SD-001@19	218	2	15	0.011	0.52210	2.42	0.0661	1.51	0.62292	411.6	6.1
10SD-001@2	126	3	9	0.026	0.52388	3.06	0.0684	1.55	0.50651	426.3	6.5
10SD-001@20	179	45	13	0.250	0.46681	3.31	0.0628	1.51	0.45678	393.2	5.9
10SD-001@21	273	125	21	0.457	0.51872	2.21	0.0653	1.51	0.68038	406.5	6.0
10SD-001@22	361	213	33	0.591	0.58938	2.65	0.0748	1.52	0.57273	464.7	6.9
10SD-001@23	123	62	11	0.504	0.53170	4.48	0.0724	1.52	0.33862	452.2	6.8
10SD-001@26	116	39	9	0.335	0.46799	3.57	0.0646	1.51	0.42177	404.5	6.0
10SD-001@4	149	10	10	0.064	0.52031	3.21	0.0640	1.57	0.48714	397.5	6.2
10SD-001@5	2403	1156	205	0.481	0.54366	1.70	0.0706	1.50	0.88396	439.5	6.5
10SD-001@6	487	89	36	0.182	0.51588	2.33	0.0670	1.51	0.64613	417.5	6.2
10SD-001@7	283	2	20	0.008	0.53911	5.08	0.0682	1.50	0.29616	424.0	6.5
10SD-001@8	136	53	10	0.389	0.47426	4.65	0.0617	1.52	0.32591	385.2	5.8
10SD-001@9	12,092	723	1037	0.060	0.61682	1.53	0.0798	1.50	0.98071	495.6	7.3
10SD-001@14	200	118	51	0.590	2.44801	1.75	0.1994	1.50	0.85998	1157.1	17.0
10SD-001@17	569	196	86	0.345	1.39803	2.28	0.1327	2.13	0.93210	792.5	16.4
10SD-001@3	405	283	78	0.699	1.43066	1.71	0.1508	1.50	0.87794	905.7	13.2
Grt-bearing leucosome											
3-5@12	254	82	19	0.323	0.48820	2.44	0.0636	1.51	0.61825	397.1	5.9
3-5@1	312	107	23	0.342	0.47556	2.09	0.0637	1.50	0.71644	398.5	5.9
3-5@15	287	110	22	0.383	0.48631	2.55	0.0647	1.92	0.75368	404.1	7.6
3-5@9	403	169	31	0.419	0.49643	1.86	0.0649	1.51	0.81567	405.2	6.0
3-5@8	229	92	18	0.400	0.48907	2.42	0.0652	1.50	0.62106	407.5	6.0
3-5@7	503	228	39	0.453	0.50198	1.94	0.0653	1.52	0.78245	407.1	6.1
3-5@10	223	50	16	0.222	0.49879	2.41	0.0655	1.53	0.63702	408.8	6.2
3-5@14	222	68	17	0.305	0.50159	2.16	0.0658	1.50	0.69451	410.5	6.1
3-5@2	299	89	23	0.297	0.50835	1.91	0.0660	1.50	0.78702	411.2	6.1
3-5@3	249	83	19	0.335	0.50177	2.10	0.0664	1.50	0.71479	414.7	6.1
3-5@18	543	230	43	0.424	0.50397	1.80	0.0668	1.50	0.83769	417.4	6.2
3-5@11	258	82	20	0.316	0.50231	1.99	0.0672	1.50	0.75324	419.7	6.2
3-5@17	249	80	19	0.322	0.50788	1.96	0.0672	1.50	0.76538	419.4	6.2
3-5@16	297	97	23	0.327	0.51445	1.88	0.0675	1.50	0.79664	420.9	6.2
3-5@6	1032	307	80	0.298	0.50923	1.63	0.0675	1.50	0.92128	421.2	6.2
3-5@5	381	120	30	0.316	0.50519	2.51	0.0681	1.50	0.59853	425.8	6.3
3-5@13	263	85	21	0.322	0.52437	1.95	0.0682	1.51	0.77091	425.4	6.3
Grt-free leucosome											
6-3@9	1892	258	142	0.136	0.52172	1.57	0.0685	1.50	0.95641	427.0	6.3
6-3@8	815	66	61	0.081	0.51824	1.66	0.0688	1.50	0.90621	429.6	6.3
6-3@7	546	34	40	0.062	0.51065	1.76	0.0678	1.50	0.85336	423.5	6.2
6-3@6	709	47	52	0.067	0.51533	1.83	0.0676	1.50	0.82104	421.6	6.2
6-3@5	539	27	39	0.050	0.51899	1.74	0.0684	1.50	0.86237	426.4	6.3
6-3@4	2038	302	155	0.148	0.52441	1.57	0.0692	1.50	0.95845	431.7	6.4
6-3@3	1926	261	142	0.135	0.51594	1.62	0.0672	1.50	0.92607	419.0	6.2
6-3@2	3075	389	223	0.127	0.50571	1.58	0.0663	1.54	0.97226	413.6	6.3
6-3@18	506	36	36	0.071	0.50488	1.78	0.0668	1.51	0.84775	417.2	6.2
6-3@17	1487	137	112	0.092	0.52794	1.59	0.0698	1.50	0.94624	435.3	6.4
6-3@16	1188	125	90	0.105	0.52657	1.65	0.0694	1.55	0.93595	432.6	6.6
6-3@15	1592	170	117	0.107	0.51242	1.60	0.0674	1.51	0.94069	420.7	6.2
6-3@14	1594	169	120	0.106	0.52838	1.59	0.0693	1.50	0.94702	431.8	6.4
6-3@13	869	77	66	0.088	0.52957	1.65	0.0696	1.50	0.91013	434.1	6.4
6-3@12	1154	124	85	0.107	0.51856	1.66	0.0681	1.50	0.90507	424.5	6.3
6-3@11	1513	174	109	0.115	0.50354	1.66	0.0660	1.50	0.90169	411.5	6.1
6-3@10	726	66	53	0.091	0.51002	1.71	0.0674	1.50	0.87979	420.6	6.2
6-3@1	1480	142	111	0.096	0.53228	1.60	0.0691	1.50	0.93845	430.4	6.3

The modeled composition of the melt at 20 kbar and 800 °C is as follows: SiO_2, 70.00 wt.%, Al_2O_3, 17.39 wt.%, CaO, 1.93 wt.%, MgO, 0.28 wt.%, Fe_2O_3, 0.47 wt.%, K_2O, 4.36 wt.%, Na_2O, 5.57 wt.%. While at lower *P–T* conditions of 15 kbar and 720 °C, the modeled melt has a slightly different composition of SiO_2, 72.20 wt.%, Al_2O_3, 16.46 wt.%, CaO, 0.94 wt.%, MgO, 0.15 wt.%, Fe_2O_3, 0.35 wt.%, K_2O, 2.76 wt.%, Na_2O, 7.14 wt.%. These latter values are roughly consistent with the bulk composition of the Grt-free leucosomes (Table 2). The decreased concentrations of MgO, Fe_2O_3, and Al_2O_3 are likely caused by the cumulate removal of garnet. Therefore, the Grt-free leucosome composition should represent a melt that originated in equilibrium with garnet. During the later decompression, hornblendic amphibole would overprint the rocks, transforming the host rocks into garnet amphibolite (or amphibolitized eclogite due to incomplete re-equilibration).

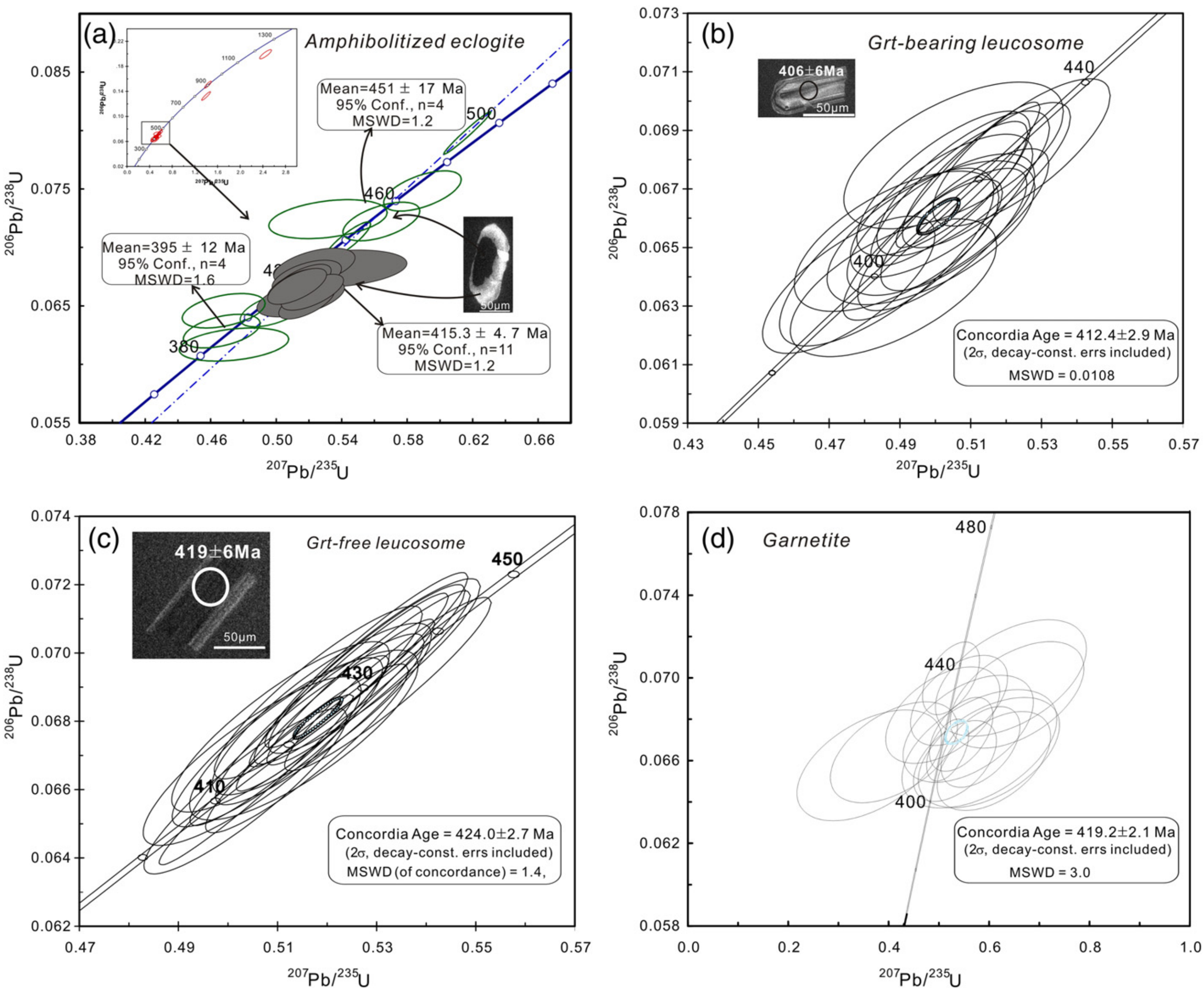

Fig. 7. Concordia diagrams showing results of the zircon U–Pb data from the amphibolitized eclogite (a), Grt-bearing leucosome (b), and Grt-free leucosome (c), and garnetite (d) from South Dulan, North Qaidam UHPM belt, China. Data-point error ellipses are 2σ.

Table 4
U, Th and Pb LA-ICP-MS zircon data of garnetite, South Dulan, North Qaidam UHPM belt, China.

Sample/spot #	[U] ppm	[Th] ppm	[Pb] ppm	Th/U meas	$^{207}Pb/^{235}U$	±1σ	$^{206}Pb/^{238}U$	±1σ	207-corr age (Ma)	±1σ
Garnetite										
G1-01	148	64	46	0.432	0.53212	0.05449	0.06598	0.00129	411.9	7.8
G1-03	122	53	40	0.431	0.54025	0.0638	0.06891	0.00144	429.6	8.7
G1-06	72	12	22	0.169	0.58078	0.10184	0.06657	0.00189	415.5	11.5
G1-07	84	24	26	0.287	0.59967	0.09288	0.06639	0.00176	414.4	10.6
G1-11	80	22	26	0.274	0.64336	0.09929	0.07	0.00186	436.2	11.2
G1-12	154	76	49	0.492	0.58281	0.05192	0.06666	0.00129	416	7.8
G1-13	106	34	33	0.318	0.60954	0.07458	0.06598	0.00158	411.9	9.6
G1-15	229	83	75	0.363	0.52424	0.03743	0.06998	0.00116	436	7.0
G1-19	98	19	31	0.196	0.65574	0.08789	0.06918	0.0017	431.2	10.3
G1-20	114	49	36	0.427	0.50778	0.07511	0.0682	0.00154	425.3	9.3
G1-26	98	35	31	0.355	0.55831	0.08562	0.06754	0.00171	421.3	10.3
G1-27	101	41	31	0.405	0.41047	0.08356	0.0664	0.00161	414.4	9.8
G1-28	82	12	26	0.143	0.81771	0.1043	0.06735	0.00191	420.2	11.5
G1-29	351	250	113	0.712	0.51743	0.02761	0.06651	0.00099	415.1	6.0
G1-30	211	90	66	0.426	0.54445	0.04174	0.06727	0.00118	419.7	7.1

Table 5
Zircon Lu–Hf isotopic data for the Grt-free leucosome, South Dulan, North Qaidam UHPM belt, China.

Spots	$^{176}Yb/^{177}Hf$	$^{176}Lu/^{177}Hf$	$^{176}Hf/^{177}Hf$	2σ	f_{DM}	$^{176}Hf/^{177}Hf$	$\varepsilon_{Hf}(0)$	ε_{Hf}(424 Ma)	2σ	T_{DM1} (Ma)	2σ	T_{DM2} (Ma)	2σ
6-3-02	0.001890	0.000032	0.282433	0.000018	0.156627	0.282433	−12.0	−2.7	0.6	1130	49	1585	80
6-3-03	0.003429	0.000053	0.282520	0.000019	0.156627	0.282520	−8.9	0.4	0.7	1011	52	139	86
6-3-04	0.001384	0.000022	0.282449	0.000015	0.156627	0.282449	−11.4	−2.1	0.5	1107	40	1549	66
6-3-05	0.000756	0.000012	0.282419	0.000021	0.156627	0.282418	−12.5	−3.2	0.7	1149	56	1618	92
6-3-06	0.002819	0.000040	0.282369	0.000017	0.156627	0.282368	−14.3	−5.0	0.6	1218	47	1729	77
6-3-07	0.002162	0.000033	0.282416	0.000020	0.156627	0.282416	−12.6	−3.3	0.7	1153	56	1623	91
6-3-08	0.000827	0.000013	0.282407	0.000018	0.156627	0.282407	−12.9	−3.6	0.6	1165	49	1643	81
6-3-09	0.003184	0.000072	0.282439	0.000027	0.156627	0.282438	−11.8	−2.5	1.0	1123	75	1573	122
6-3-10	0.001600	0.000030	0.282425	0.000023	0.156627	0.282425	−12.3	−3.0	0.8	1140	62	1603	102
6-3-11	0.001185	0.000021	0.282420	0.000020	0.156627	0.282420	−12.5	−3.1	0.7	1148	55	1615	90
6-3-12	0.001096	0.000020	0.282428	0.000015	0.156627	0.282428	−12.1	−2.8	0.5	1136	41	1595	67
6-3-14	0.001727	0.000029	0.282431	0.000015	0.156627	0.282430	−12.1	−2.8	0.5	1133	40	1591	66
6-3-16	0.001913	0.000029	0.282453	0.000017	0.156627	0.282453	−11.3	−2.0	0.6	1102	45	1540	74
6-3-17	0.002650	0.000040	0.282428	0.000017	0.156627	0.282428	−12.2	−2.9	0.6	1137	47	1596	77
6-3-18	0.001902	0.000033	0.282381	0.000014	0.1566	0.282381	−13.8	−4.5	0.5	1200	38	1701	63
6-3-21	0.001275	0.000025	0.282420	0.000023	0.156627	0.282420	−12.4	−3.1	0.8	1147	64	1614	105
6-3-23	0.000927	0.000014	0.282438	0.000017	0.156627	0.282438	−11.8	−2.5	0.6	1123	46	1575	76
6-3-24	0.001853	0.000040	0.282459	0.000017	0.156627	0.282459	−11.1	−1.8	0.6	1094	45	1527	74
6-3-25	0.001023	0.000019	0.282422	0.000022	0.156627	0.282422	−12.4	−3.1	0.8	1144	59	1609	96

8. Discussion

8.1. Igneous garnet and partition coefficients with melt

Distinguishing the original protolith garnet from a metamorphic reaction product through major elemental compositions alone is often difficult (Clarke et al., 2013). Garnet in the amphibolitized eclogite of this study, which has a typical metamorphic origin, preserves the zonation profile for the major elements, particularly Fe, Mg and Ca (Fig. 3a, Table 1), while Mn is distributed much more uniformly possibly due to homogenization during the granulite-facies overprinting (Table 1). However, the trace elements are homogeneous from core to rim for these eclogitic garnets. In contrast, the garnet in garnetite is homogeneous for the major elements but displays obvious zonation from core to rim in the REE pattern (Fig. 4c). The more compatible HREE decrease markedly from core to rim, while the incompatible LREE increase slightly. The combination of constant major elements with this trace element profile can be explained if the garnets grew from a partial melt whose major element composition was buffered by coexisting solid phases, while trace element content followed Rayleigh fractionation trends due to efficient physical removal of garnet from the melt (cf. Otamendi et al., 2002), consistent with the deductions of Song et al. (2014a) and other observations in the current study. Therefore, the coexisting garnetite and leucosome melt provide an opportunity to examine trace element partition coefficients between the garnet in the garnetite and the melt as represented by the coexisting garnet-free leucosome. The rim composition of the garnet was used in this calculation. Appendix B presents the data used to calculate the partition coefficients for the trace elements. The calculated garnet/melt partition coefficients ($D_{Grt/melt}$) compare well with experimentally determined partition coefficients (Xiong, 2006) in Fig. 4d. The *D* values for HREE are the highest, followed by those of the transition elements and HFSE; however, the LILE and LREE *D* values are lowest (<0.01). Thus, the derived partition coefficients are consistent with our hypothesis that the garnetite is a cumulate, whose garnets originate from adakitic melt at high pressure (Song et al., 2014a). This is also consistent with the above phase modeling result of the decreased concentrations of MgO, Fe_2O_3, and Al_2O_3 caused by the cumulate removal of garnet along with the melt composition evolution.

8.2. The role of Ti-rich phases during partial melting

In this study, two generations of rutile were recognized in the Grt-bearing and Grt-free leucosome melts (Fig. 3b, c). The relict rutile (Rt_1) has the same grain size and rounded shape as the rutile in the amphibolitized eclogite (Fig. 3a), while the rare neocryst rutile (Rt_2) is more euhedral. The relict rutile may have been inherited from the eclogite precursor, while the new rutile may be the product of rapid crystallization that occurred as the leucosome melt cooled. Experimental studies have indicated that titanium diffuses very rapidly in hydrous melts (Hayden and Watson, 2007). Rutile and other Ti-rich accessory phases are always denser than the coexisting melt, and the viscosity of a hydrous melt is quite low. Therefore, it is possible that Ti-rich phases separate from the hydrous melt very quickly and remain in the residue

Table 6
Trace element budget based on mineral modal abundances and representative trace elemental contents for the minerals in the garnetite.

Modal	Grt	Ab	Ttn	Ep	Rt	Zrc	Estimated total	Bulk rock
	0.84	0.1	0.055	0.005	0.0042	0.0004	From mineral abundances	
TiO2	0.86	0.03	35.4	0.20	100		3.08	3.08
Nb	3.61	0.04	127	0.11	2786		21.63	23
Ta	0.30	0.02	10.9	<0.032	298		2.09	2.2
W	0.45	<0.059	1.10	2.62	284		1.64	2
Sb	0.11	<0.069	0.05	3.94	1.55		0.12	
Mo	0.24	<0.097	4.82	0.35	30.78		0.60	2
Sn	1.35	0.76	32.7	15.52	218.74		3.99	5
Zr	60	0.25	312	22.53	614.86	491,000	251	251
Hf	2.48	0.03	11.3	1.19	18.29	8000	5.7	5.7
Cr	6.35	4.68	5.92	138.8	25.38		6.92	10
ΣLREE	2.96	3.89	3151	52,057			436.4	449.6
ΣMREE	66	0.59	251	1691			77.34	76.33
ΣHREE	28		32	101			25.79	25.29

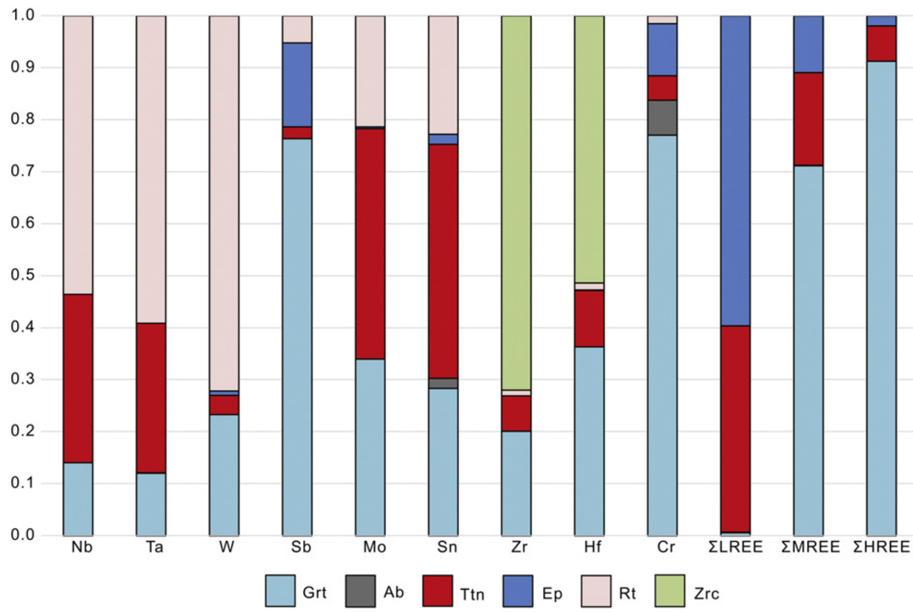

Fig. 8. Mass balance calculations for HFSE distributions among different major mineral phases in the garnetite from South Dulan, North Qaidam UHPM belt, China.

during/after partial melting (Xiong et al., 2009). The enrichment in titanite observed for the garnetite cumulate is consistent with this idea. In contrast, the presence of relict rutile in the leucosomes possibly indicates that the melt has not moved far from the source. Compositionally, the relict rutile has the same trace element composition as the neocryst rutile, but different from the rutile in the eclogite precursor (Fig. 5), implying that the relict rutile might be re-equilibrated with the surrounding melts.

To quantify the distributions of HFSE between the different minerals of the garnetite, we performed a trace element mass balance analysis similar to that used in other studies such as Zack et al. (2002). Elemental mapping and XRF whole-rock data were applied to estimate the rutile and titanite concentrations in the garnetite. We chose the coarse-grained and homogeneous portions with weighted mean trace element concentrations of the mineral phases used. The modal abundances of minerals in the garnetite are listed in Table 6, and the calculated abundances of Nb, Ta, W, Ti, Sb, Sn, Mo, Cr, Zr, Hf and REE between major mineral phases are shown in Fig. 8. As mentioned above, rutile inclusions are always present in garnet, especially the garnet core, so care was taken to avoid rutile inclusions in our analysis. Of the analyzed phases, rutile shows the strongest preference for HFSE, particularly for Nb and Ta, which are consistent with observations elsewhere (e.g., Zack et al., 2002) (Fig. 8). However, when titanite occurs as a coexisting phase, it competes with rutile for these elements, incorporating about half of the amount of Nb and Ta that rutile does (Fig. 8). Most of the LREE (La–Nd) are incorporated into titanite and epidote, while garnet incorporates most MREE (Sm–Ho + Y) and HREE (Er–Lu) (Fig. 8). Therefore, the garnet and Ti-rich phases (rutile and titanite) in the cumulate garnetite play an important role in producing the stronger adakitic signature in the Grt-free leucosome melts (Table 2), and perhaps also the adakitic signature of the nearby tonalite pluton (Song et al., 2014a).

8.3. P–T–t evolution through the partial melting process

The eclogites most likely experienced UHP conditions, based on the coesite inclusions in the same terrane (J.X. Zhang et al., 2010) and conventional thermobarometric calculations (Song et al., 2003a) (Fig. 9). Some eclogitic zircon cores record an eclogite-facies metamorphic age of 451 ± 17 Ma (Fig. 7a), similar to the data of J.X. Zhang et al. (2010). These zircons might record an early age of oceanic subduction (Song et al., 2014b; Zhang et al., 2013). In the three eclogite terranes (Yuka, Xitieshan and Dulan), UHP metamorphism occurred at around 440–430 Ma (Song et al., 2014b; Zhang et al., 2013). During the initial exhumation stage, the eclogite appears to follow a decompression path with a slight temperature increase; decompression triggered partial melting when the rocks crossed the solidus in Fig. 9 at ~20 kbar, 800 °C (~60 km, Song et al., 2014a). A low degree of partial melting (~10%) generated the first silica-rich melts (Grt-free leucosome in Fig. 2). Zircons in the leucosome crystallized between 434.1 ± 6.4 Ma and 411.5 ± 6.1 Ma, with a mean age of 424.0 ± 2.7 Ma (Table 3, Fig. 7c). The relatively early growth of zircon may reflect overgrowth on pre-existing larger zircons fed by dissolution of small zircons, i.e. Ostwald ripening, in the presence of melt (Vavra et al., 1999) rather than nucleation in the melt. In view of the comparatively high solubility of U and low solubility of Th in H_2O, the relatively low Th/U ratios of 0.067 to 0.148 in zircon (Table 3) may indicate that this zircon crystallized from a H_2O-rich parent magma (in this case, the Grt-free leucosome).

During cooling, garnet crystallized from and equilibrated with these melts to form the garnetite cumulate layer (419.2 ± 2.1 Ma, 15 kbar and 720 °C). The melt accumulated to form in-situ melt patches within the eclogite and moved only a limited distance, based on the persistence of their relict rutile. As these Grt-free leucosome melts crystallized, they interacted with the country eclogite again to produce silica-poor melts at 412.4 ± 2.9 Ma, which are observed as Grt-bearing leucosomes (Fig. 9). Compared with the Grt-free leucosome, these later melts have lower U contents of 222–543 ppm and higher Th/U ratios of 0.297–0.653, and are deduced to have been less hydrous than the Grt-free leucosome melts (Table 3).

For eclogite, a mean age of 415.3 ± 4.7 Ma recorded by zircon rims and a few neocrystallized zircon grains is effectively synchronous with the generation of Grt-bearing leucosome (Fig. 7a). Subsequently, all rock types experienced later amphibolite-facies retrogression at ~400 Ma based on the amphibolitized eclogite (Fig. 9).

8.4. Implications for adakite genesis

As discussed by Song et al. (2014a), granulite residue, leucosome and a tonalite pluton near the outcrop of this study in the South Dulan terrane show depleted Sr, Nd and Hf isotope signatures, suggesting that oceanic crust was the proposed melt source. In this study, however, the older (>700 Ma) inherited zircon core protolith ages preserved in

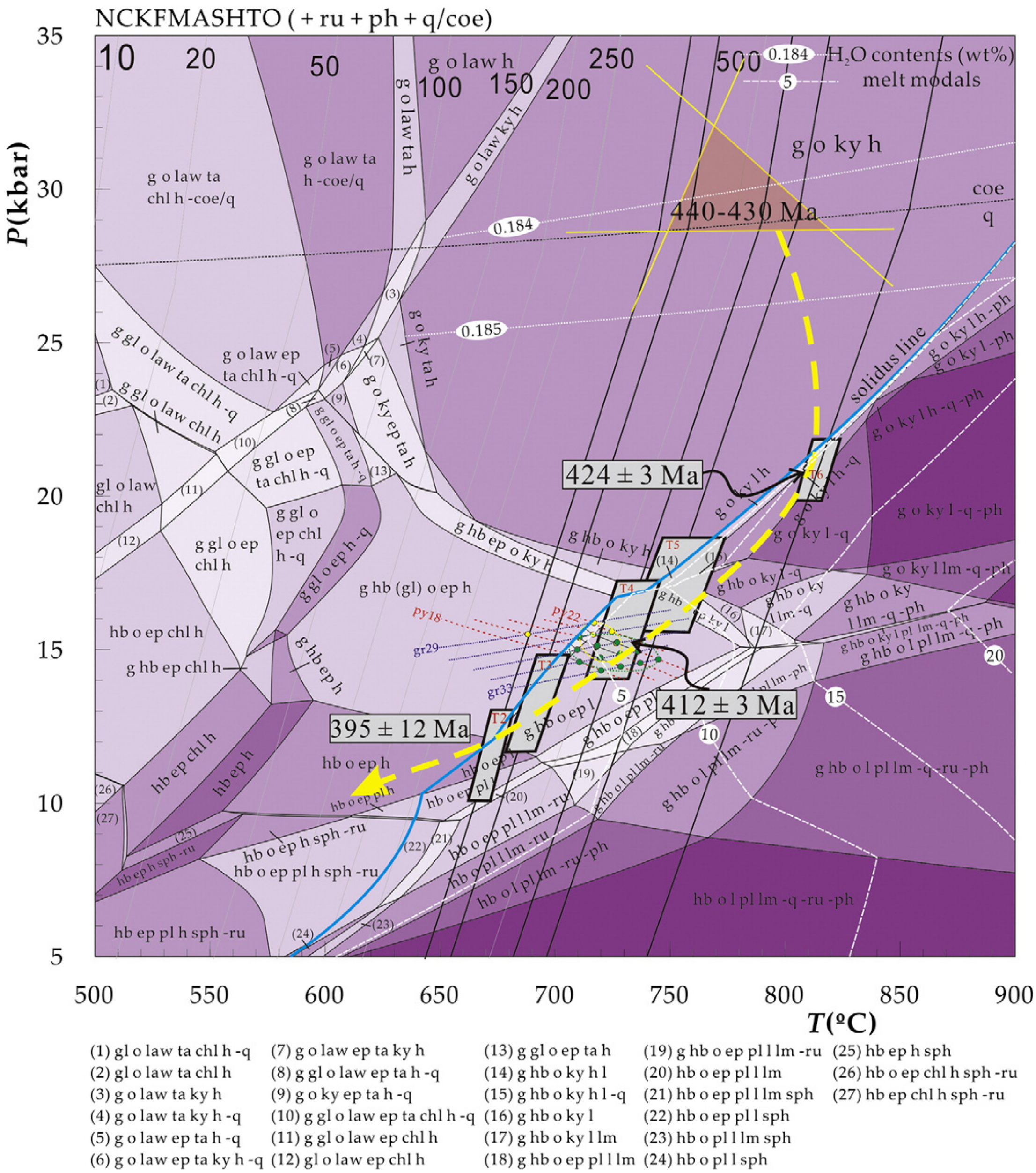

Fig. 9. *P–T–*t path deduced from the pseudosection calculations using the eclogite compositions, the contoured Zr-in-rutile thermobarometry, and zircon U–Pb age data from the amphibolitized eclogite and leucosomes. *P–T* conditions for the eclogite facies condition follow Song et al. (2003a). Mineral abbreviations: g, garnet; o, omphacite; law, lawsonite; chl, chlorite; h, hornblende; q, quartz; ep, epidote; gl, glaucophane; pl, plagioclase; ru, rutile; sph, sphene; ph, phengite. The parallelograms labeled T2 to T6 along the Zr-in-rutile contour lines represent the thin Sections 2 to 6 in Fig. 2b.

the amphibolitized eclogite investigated here (Fig. 7a) are similar to previous results (~835 Ma, J.X. Zhang et al., 2010). A Neoproterozoic continental rift or incipient oceanic basin setting has been proposed as the tectonic setting for the protoliths, which subsequently were subducted with the continental rocks in the early Paleozoic, undergoing UHP metamorphism and tectonic emplacement into the continental crust (Chen et al., 2009; J.X. Zhang et al., 2010). The negative values of ε_{Hf} (424 Ma) (−5.0 to 0.4) of the Grt-free leucosome melts reflect an enriched Hf isotopic composition signature (Wu et al., 2007). Combined with the old model ages (T_{DM1} > 1000 Ma, Table 5), these data indicate partial melting of the exhumed continental rocks. Therefore, both oceanic and continental rocks were partially melted during exhumation. For the early stage, decompression triggered the partial melting of garnet and omphacite during the transition from eclogite- to granulite-facies conditions (Song et al., 2014a). Then, for the late stage, the continental lower crust was also partially melted to produce the observed outcrop of this study (Fig. 2).

Typical adakite and Archean TTG are silicic to intermediate igneous rocks, geochemically characterized by high Al_2O_3, Ni, and Cr contents, high $Mg^{\#}$ and Sr/Y ratios, steep REE patterns and strong depletion of HFSE (Martin et al., 2005). The leucosome melts in this study share general features with slab-derived adakitic melts (Song et al., 2014a; Yu et al., 2011 and this study). Experiments indicate that partial melts in equilibrium with <20 wt.% plagioclase will be enriched in Sr, while >20 wt.% garnet will elevate the La/Yb ratio (Qian and Hermann, 2013). Igneous garnet readily incorporates Y and HREE such as Yb, and by fractionating to form a garnetite cumulate, depletes the Y and Yb concentrations in the Grt-free leucosome. Concurrently, because the garnetite is plagioclase-poor, Sr is enriched in the leucosome melts. Hence, the Grt-free leucosome melts develop a very strong adakitic signature of extremely high Sr/Y (>5000) and $(La/Yb)_N$ (>200) ratios (Table 2). The garnet crystallized from melt in the second episode of partial melting does not separate as a cumulate phase. Therefore, Grt-bearing leucosomes show a less extreme adakitic signature in their Sr/Y (179–294) and $(La/Yb)_N$ (234–476) ratios (Table 2).

Analysis of the *P*–*T*–t path and pseudosection construction indicates that tonalitic–trondhjemitic/adakitic melts were generated in two distinct episodes. Decompression partial melting under higher pressure conditions (~20 kbar) generated the early hydrous melts at ~425 Ma, which physically separated into Grt-free leucosome and garnetite, while under lower pressure conditions (<15 kbar) at ~415 Ma, a second episode of melts were generated which retained their garnet. *P*–*T* conditions for the latter are similar to those in the experiments of Qian and Hermann (2013).

9. Conclusions

1) Two episodes of partial melting occurred during exhumation of the South Dulan eclogite in the North Qaidam UHPM belt. The first generation of Grt-free leucosome melts formed through decompression melting of the eclogite at 424.0 ± 2.7 Ma. The zircon compositions indicate that the melts were hydrous. The second episode of Grt-bearing leucosome melts crystallized at 415.3 ± 4.7 Ma, and these melts were less hydrous.
2) Rutile is difficult to dissolve in the melt, but it could be re-equilibrated. These crystals account for the unusual enrichment of Nb and Ta in the leucosome melts. The rutile and titanite in the garnetite cumulate control the distribution of the high field strength elements (HFSE) during partial melting.
3) The *P*–*T*–t path deduced from the Zr-in-rutile thermometry and pseudosection calculation indicates that the igneous garnet accumulated from the melts under high pressure. The igneous garnet has a strong REE zoning, and its removal accounts for the extremely strong adakitic signature of the tonalitic–trondhjemitic melts. Conversely, the lower-pressure partial melts without garnet separation generate adakitic melts that are more usual.

Supplementary data to this article can be found online at http://dx.doi.org/10.1016/j.lithos.2014.12.009.

Acknowledgments

We thank Dr. Fang Ma for her help with the LA-ICP-MS analysis, Dr. Chunli Guo help with the Hf isotope analysis, Dr. Zhenyu Chen help with EMP analysis. We also thank Prof. Chunjing Wei for discussion of the manuscript. Profs. Daniele Castelli and Gordon Medaris and two other anonymous reviewers are thanked for their constructive reviews of this paper. This study was supported by the Major State Basic Research Development Program (Grants 2015CB856105 and 2009CB825007), National Natural Science Foundation of China (Grants 41272068, 41090371, 41121062 and 41330210), the Program for New Century Excellent Talents in University (NCET-13-0017), foundation of MLR Key Laboratory of Metallogeny and Mineral Assessment (ZS1303) and Instrumental Analysis Fund of Peking University.

References

Andersen, T., 2002. Correction of common lead in U–Pb analyses that do not report ^{204}Pb. Chemical Geology 192, 59–79.
Audétat, A., Keppler, H., 2005. Solubility of rutile in subduction zone fluids, as determined by experiments in the hydrothermal diamond anvil cell. Earth and Planetary Science Letters 232, 393–402.
Auzanneau, E., Vielzeuf, D., Schmidt, M.W., 2006. Experimental evidence of decompression melting during exhumation of subducted continental crust. Contributions to Mineralogy and Petrology 152, 125–148.
Castillo, P.R., 2006. An overview of adakite petrogenesis. Chinese Science Bulletin 51, 257–268.
Castillo, P.R., 2012. Adakite petrogenesis. Lithos 134–135, 304–316.
Chen, D.L., Liu, L., Sun, Y., Liou, J.G., 2009. Geochemistry and zircon U–Pb dating and its implications of the Yukahe HP/UHP terrane, the North Qaidam, NW China. Journal of Asian Earth Sciences 35, 232–244.
Clarke, G.L., Daczko, N.R., Miescher, D., 2013. Identifying relic igneous garnet and clinopyroxene in eclogite and granulite, Breaksea Orthogneiss, New Zealand. Journal of Petrology 54, 1921–1938.
Coggon, R., Holland, T.J.B., 2002. Mixing properties of phengitic micas and revised garnet-phengite thermobarometers. Journal of Metamorphic Geology 20, 683–696.
Diener, J.F.A., Powell, R., White, R.W., Holland, T.J.B., 2007. A new thermodynamic model for clino- and orthoamphiboles in the system Na_2O–CaO–FeO–MgO–Al_2O_3–SiO_2–H_2O–O. Journal of Metamorphic Geology 25, 631–656.
Drummond, M.S., Defant, M., 1990. A model for trondhjemite–tonalite–dacite genesis and crustal growth via slab melting: Archean to modern comparisons. Journal of Geophysical Research 95, 21503–21521.
Ellis, D.J., Green, D.H., 1979. An experimental study of the effect of Caupon garnet–clinopyroxene Fe–Mg exchange equilibria. Contributions to Mineralogy and Petrology 71, 13–22.
Foley, S.F., Barth, M.G., Jenner, G.A., 2000. Rutile/melt partition coefficients for trace elements and an assessment of the influence of rutile on the trace element characteristics of subduction zone magmas. Geochimica et Cosmochimica Acta 5, 933–938.
Foley, S.F., Tiepolo, M., Vannucci, R., 2002. Growth of early continental crust controlled by melting of amphibolite in subduction zones. Nature 417, 837–840.
Gou, L.L., Zhang, L.F., Tao, R.B., Du, J.X., 2012. A geochemical study of syn-subduction and post-collisional granitoids at Muzhaerte River in the Southwest Tianshan UHP belt, NW China. Lithos 136–139, 201–224.
Green, T.H., 2000. New partition coefficient determinations pertinent to hydrous melting processes in subduction zones. In: Davidson, J.P., Davidson, J.A., Price, R.C. (Eds.), State of the Arc 2000: Processes and Timescales. Carolyn Bain Publishing House, Wellington, pp. 92–95.
Green, T.H., Adam, J., 2003. Experimentally-determined trace element characteristics of aqueous fluid from partially dehydrated mafic oceanic crust at 3.0 GPa, 650–700 °C. European Journal of Mineralogy 15, 815–830.
Green, T.H., Pearson, N.J., 1987. An experimental study of Nb and Ta partitioning between Ti-rich minerals and silicate liquids at high pressure and temperature. Geochimica et Cosmochimica Acta 51, 55–62.
Green, E., Holland, T., Powell, R., 2007. An order–disorder model for omphacitic pyroxenes in the system jadeite–diopside–hedenbergite–acmite, with applications to eclogitic rocks. American Mineralogist 92, 1181–1189.
Hawthorne, F.C., Oberti, R., Harlow, G.E., Maresch, W.V., Martin, R.F., Schumacher, J.C., Welch, M.D., 2012. Nomenclature of the amphibole supergroup. American Mineralogist 97, 2031–2048.
Hayden, L.A., Watson, B.E., 2007. Rutile saturation in hydrous siliceous melts and its bearing on Ti-thermometry of quartz and zircon. Earth and Planetary Science Letters 258, 561–568.
Holland, T.J.B., Powell, R., 1998. An internally consistent thermodynamic data set for phases of petrological interest. Journal of Metamorphic Geology 16, 309–343.
Holland, T., Powell, R., 2003. Activity–composition relations for phases in petrological calculations: an asymmetric multicomponent formulation. Contributions to Mineralogy and Petrology 145, 492–501.
Holland, T., Baker, J., Powell, R., 1998. Mixing properties and activity–composition and relationships of chlorites in the system MgO–FeO–Al_2O_3–SiO_2–H_2O. European Journal of Mineralogy 10, 395–406.
Hou, K.J., Li, Y.H., Zou, T.R., Qu, X.M., Shi, Y.R., Xie, G.Q., 2007. Laser ablation-MC-ICP-MS technique for Hf isotope microanalysis of zircon and its geological applications. Acta Petrologica Sinica 23, 2595–2604.
Kohn, M.J., Spear, F.S., 1990. Two new geobarometers for garnet amphibolites, with applications to southeastern Vermont. American Mineralogist 75, 89–96.
Kretz, R., 1983. Symbols for rock-forming minerals. American Mineralogist 68, 277–279.
Krogh Ravna, E., Terry, M.P., 2001. Geothermobarometry of phengite–Kyanite–quartz/coesite eclogites. Eleventh Annual V.M. Goldschmidt Conference, Abstract #3145. LPI Contribution No. 1088. Lunar and Planetary Institute, Houston (CD Rom).
Labrousse, L., Prouteau, G., Ganzhorn, A.C., 2011. Continental exhumation triggered by partial melting at ultrahigh pressure. Geology 39, 1171–1174.
Li, X.H., Liu, Y., Li, Q.L., Guo, C.H., Chamberlain, K.R., 2009. Precise determination of Phanerozoic Zircon Pb/Pb age by multicollector SIMS without external standardization. Geochemistry, Geophysics, Geosystems 10, 4.
Ludwig, K.R., 2002. SQUID 1.02, a user's manual. Berkeley Geochronology Center Special Publication 2 p. 22 (2455 Ridge Road, Berkeley, CA 94709, USA).
Ludwig, K.R., 2003. User's manual for Isoplot 3.00: a geochronological toolkit for Microsoft Excel. Berkeley Geochronology Center Special Publication 4 p. 70 (Berkeley).
Manning, C.E., Wilke, M., Schmidt, C., Cauzid, J., 2008. Rutile solubility in albite–H_2O and $Na_2Si_3O_7$–H_2O at high temperatures and pressures by in-situ synchrotron radiation micro-XRF. Earth and Planetary Science Letters 272, 730–737.
Martin, H., Smithies, R.H., Rapp, R., Moyen, J.F., Champion, D., 2005. An overview of adakite, tonalite–trondhjemite–granodiorite (TTG), and sanukitoid: relationships and some implications for crustal evolution. Lithos 79, 1–24.
Niu, Y.L., 2004. Bulk-rock major and trace element compositions of abyssal peridotites: implications for mantle melting, melt extraction and post-melting processes beneath ocean ridges. Journal of Petrology 45, 2423–2458.
Otamendi, J.E., de la Rosa, J.D., Patino Douce, A.E., Castro, A., 2002. Rayleigh fractionation of heavy rare earths and yttrium during metamorphic garnet growth. Geology 30, 159–162.
Pearce, N.J.G., Perkins, W.T., Westgate, J.A., Gorton, M.P., Jackson, S.E., Neal, C.R., Chenery, S.P., 1997. A compilation of new and published major and trace element data for NIST SRM 610 and NIST SRM 612 glass reference materials. Geostandards Newsletter 21, 115–144.
Powell, R., 1985. Regression diagnostics and robust regression in geothermometer/geobarometer calibration: the garnet–clinopyroxene geothermometer revisited. Journal of Metamorphic Geology 3, 231–232.

Powell, R., Holland, T., Worley, B., 1998. Calculating phase diagrams involving solid solutions via non-linear equations, with examples using THERMOCALC. Journal of Metamorphic Geology 16, 577–588.

Qian, Q., Hermann, J., 2013. Partial melting of lower crust at 10–15 kbar: constraints on adakite and TTG formation. Contributions to Mineralogy and Petrology 165, 1195–1224.

Rapp, R.P., Watson, E.B., Miller, C.F., 1991. Partial melting of amphibolite/eclogite and the origin of Archean trondhjemites and tonalites. Precambrian Research 51, 1–25.

Rapp, R.P., Shimizu, N., Norman, M.D., 2003. Growth of early continental crust by partial melting of eclogite. Nature 425, 605–609.

Sawyer, E.W., Brown, M., 2008. Working with migmatites: nomenclature for the constituent parts. In: Raeside, R. (Ed.), Working with Migmatites vol. 38. Mineralogical Association of Canada, Quebec.

Schmidt, A., Weyer, S., John, T., Brey, G.P., 2009. HFSE systematics of rutile-bearing eclogites: new insights into subduction zone processes and implications for the earth's HFSE budget. Geochimica et Cosmochimica Acta 73, 455–468.

Sláma, J., Kosler, J., Condon, D.J., Crowley, J.L., Gerdes, A., Hanchar, J.M., Horstwood, M.S.A., Morris, G.A., Nasdala, L., Norbreg, N., Schaltegger, U., Schoene, B., Tubrett, M.N., Whitehous, M.J., 2008. Plešovice zircon — a new natural reference material for U–Pb and Hf isotopic microanalysis. Chemical Geology 249, 1–35.

Song, S.G., Yang, J.S., Liou, J.G., Wu, C.L., Shi, R.D., Xu, Z.Q., 2003a. Metamorphic evolution of the coesite-bearing ultrahigh-pressure terrane in the North Qaidam, northern Tibet, NW China. Journal of Metamorphic Geology 21, 631–644.

Song, S.G., Yang, J.S., Xu, Z.Q., Liou, J.G., Shi, R.D., 2003b. Petrology, geochemistry and isotopic ages of eclogites from the Dulan UHPM terrane, the North Qaidam, NW China. Lithos 70, 195–211.

Song, S.G., Zhang, L.F., Niu, Y.L., Su, L., Jian, P., Liu, D.Y., 2005. Geochronology of diamond-bearing zircons in garnet peridotite in the North Qaidam UHPM belt, North Tibetan Plateau: a record of complex histories associated with continental collision. Earth and Planetary Science Letters 234, 99–118.

Song, S.G., Zhang, L.F., Niu, Y.L., Su, L., Song, B., Liu, D.Y., 2006. Evolution from oceanic subduction to continental collision: a case study of the Northern Tibetan Plateau inferred from geochemical and geochronological data. Journal of Petrology 47, 435–455.

Song, S.G., Niu, Y.L., Zhang, L.F., Wei, C.J., Liou, J.G., Su, L., 2009a. Tectonic evolution of Early Paleozoic HP metamorphic rocks in the North Qilian Mountains, NW China: new perspectives. Journal of Asian Earth Sciences 35, 285–297.

Song, S.G., Niu, Y.L., Zhang, L.F., Bucher, K., 2009b. The Luliang Shan garnet peridotite massif of the North Qaidam UHPM belt, NW China — a review of its origin and metamorphic evolution. Journal of Metamorphic Geology 27, 621–638.

Song, S.G., Niu, Y.L., Su, L., Wei, C.J., Zhang, L.F., 2014a. Adakitic (tonalitic–trondhjemitic) magmas resulting from eclogite decompression and dehydration melting during exhumation in response to continental collision. Geochimica et Cosmochimica Acta 130, 42–62.

Song, S.G., Niu, Y.L., Su, L., Zhang, C., Zhang, L.F., 2014b. Continental orogenesis from ocean subduction, continent collision/subduction, to orogen collapse, and orogen recycling: the example of the North Qaidam UHPM belt, NW China. Earth-Science Reviews 129, 59–84.

Stadler, R., Foley, S.F., Brey, G.P., Horn, I., 1998. Mineral–aqueous fluid partitioning of trace elements at 900–1200 °C and 3.0–5.7 GPa: new experimental data for garnet, clinopyroxene and rutile and implications for mantle metasomatism. Geochimica et Cosmochimica Acta 62, 1781–1801.

Sun, S.S., McDonough, W.F., 1989. Chemical and isotopic systematics of oceanic basalts: implications for mantle composition and processes. In: Saunders, A.D., Norry, M.J. (Eds.), Magmatism in the Ocean Basins 42. Geological Society, London, pp. 313–345.

Tomkins, H.S., Powell, R., Ellis, D.J., 2007. The pressure dependence of the zirconium-in-rutile thermometer. Journal of Metamorphic Geology 25, 703–713.

van Achterbergh, E., Ryan, C., Jackson, S.E., Griffin, W.L., 2001. Appendix 3 data reduction software for LA-ICP-MS. In: Sylvester, P. (Ed.), Laser-Ablation-ICPMS in the Earth Sciences. Mineralogical Association of Canada, Short Course, pp. 239–243.

Vavra, G., Schmid, R., Gebauer, D., 1999. Internal morphology, habit and U–Th–Pb microanalysis of amphibolite-to-granulite facies zircons: geochronology of the Ivrea Zone (Southern Alps). Contributions to Mineralogy and Petrology 134, 380–404.

Vuorinen, J.H., Hålenius, U., 2005. Nb-, Zr- and LREE-rich titanite from the Alnfalkaline complex: crystal chemistry and its importance as a petrogenetic indicator. Lithos 83, 128–142.

White, R.W., Powell, R., Holland, T.J.B., 2000. The effect of TiO_2 and Fe_2O_3 on metapelitic assemblages at greenschist and amphibolite facies conditions: mineral equilibria calculations in the system K_2O–FeO–MgO–Al_2O_3–SiO_2–H_2O–TiO_2–Fe_2O_3. Journal of Metamorphic Geology 18, 497–511.

White, R.W., Powell, R., Holland, T.J.B., 2007. Progress relating to calculation of partial melting equilibria for metapelites. Journal of Metamorphic Geology 25, 511–527.

Wu, F.Y., Zheng, Y.F., Gao, S., 2007. Lu–Hf isotopic systematics and their applications in petrology. Acta Petrologica Sinica 23 (2), 185–220.

Xiao, Y.L., Sun, W.D., Hoefs, J., Simon, K., Zhang, Z.M., Li, S.G., Hofmann, A.W., 2006. Making continental crust through slab melting: constraints from niobium–tantalum fractionation in UHP metamorphic rutile. Geochimica et Cosmochimica Acta 70, 4770–4782.

Xiao, Y.L., Huang, J., Liu, L., Li, D.Y., 2011. Rutile: an important "reservoir" for geochemical information. Acta Petrologica Sinica 27, 398–416.

Xiong, X.L., 2006. Trace element evidence for growth of early continental crust by melting of rutile-bearing hydrous eclogite. Geology 34, 945–948.

Xiong, X.L., Adam, J., Green, T.H., 2005. Rutile stability and rutile/melt HFSE partitioning during partial melting of hydrous basalt: implications for TTG genesis. Chemical Geology 218, 339–359.

Xiong, X.L., Keppler, H., Audétat, A., Gudfinnsson, G., Sun, W.D., Song, M.S., Xiao, W.S., Li, Y., 2009. Experimental constraints on rutile saturation during partial melting of metabasalt at the amphibolite to eclogite transition, with applications for TTG genesis. American Mineralogist 94, 1175–1186.

Xiong, X.L., Keppler, H., Audétat, A., Ni, H.W., Sun, W.D., Li, Y., 2011. Partitioning of Nb and Ta between rutile and felsic melt and the fractionation of Nb/Ta during partial melting of hydrous metabasalt. Geochimica et Cosmochimica Acta 75, 1673–1692.

Yang, J.J., Powell, R., 2008. Ultrahigh-pressure garnet peridotites from the devolatilization of sea-floor hydrated ultramafic rocks. Journal of Metamorphic Geology 26, 695–716.

Yang, J.S., Zhang, J.X., Meng, F.C., 2003. Ultrahigh pressure eclogites of the north Qaidam and Altun mountains, NW China and their protoliths. Earth Science Frontiers 10, 291–314 (in Chinese with English abstract).

Yin, A., Harrison, T.M., 2000. Geologic evolution of the Himalayan–Tibetan orogen. Annual Review of Earth and Planetary Sciences 28, 211–280.

Yu, S.Y., Zhang, J.X., Real, P.G., 2011. Geochemistry and zircon U–Pb ages of adakitic rocks from the Dulan area of the North Qaidam UHP terrane, north Tibet: constraints on the timing and nature of regional tectonothermal events associated with collisional orogeny. Gondwana Research 21, 167–179.

Yuan, H.L., Gao, S., Liu, X.M., Li, H.M., Günther, D., Wu, F.Y., 2004. Accurate U–Pb Age and trace element determinations of zircon by laser ablation-inductively coupled plasma-mass spectrometry. Geostandards and Geoanalytical Research 28, 353–370.

Zack, T., Kronz, A., Foley, S.F., Rivers, T., 2002. Trace element abundances in rutiles from eclogites and associated garnet mica schists. Chemical Geology 184, 97–122.

Zhang, G.B., Zhang, L.F., 2011. Rodingite from oceanic lithology of Shaliuhe terrane in North Qaidam UHPM belt and its geological implication. Earth Science Frontiers 18 (2), 151–157 (in Chinese with English abstract).

Zhang, G.B., Song, S.G., Zhang, L.F., Niu, Y.L., Shu, G.M., 2005. Ophiolite-type mantle peridotite from Shaliuhe, North Qaidam UHPM belt, NW China and its tectonic implications. Acta Petrologica Sinica 21 (4), 1049–1058 (in Chinese with English abstract).

Zhang, G.B., Song, S.G., Zhang, L.F., Niu, Y.L., 2008. The subducted oceanic crust within continental-type UHP metamorphic belt in the North Qaidam, NW China: evidence from petrology, geochemistry and geochronology. Lithos 104, 99–118.

Zhang, G.B., Zhang, L.F., Song, S.G., Niu, Y.L., 2009. UHP metamorphic evolution and SHRIMP geochronology of a coesite-bearing meta-ophiolitic gabbro in the North Qaidam, NW China. Journal of Asian Earth Sciences 35, 310–322.

Zhang, G.B., Ellis, D.J., Christy, A.G., Zhang, L.F., Song, S.G., 2010a. Zr-in-rutile thermometry in HP/UHP eclogites from Western China. Contributions to Mineralogy and Petrology 160, 427–439.

Zhang, J.X., Mattinson, C.G., Yu, S.Y., 2010b. U–Pb zircon geochronology of coesite-bearing eclogites from the southern Dulan area of the North Qaidam UHP terrane, northwestern China: spatially and temporally extensive UHP metamorphism during continental subduction. Journal of Metamorphic Geology 28, 955–978.

Zhang, G.B., Zhang, L.F., Christy, A.G., 2013. From oceanic subduction to continental collision: an overview of HP–UHP metamorphic rocks in the North Qaidam UHP belt, NW China. Journal of Asian Earth Sciences 63, 98–111.

Zhang, G.B., Zhang, L.F., Christy, A., Song, S.G., Li, Q.L., 2014. Differential exhumation and cooling history of North Qaidam UHP metamorphic rocks, NW China: constraints from zircon and rutile thermometry and U–Pb geochronology. Lithos 205, 15–27.

Zheng, Y.F., Xia, Q.X., Chen, R.X., Gao, X.Y., 2011. Partial melting, fluid supercriticality and element mobility in ultrahigh-pressure metamorphic rocks during continental collision. Earth-Science Reviews 107, 342–374.